Entanglement and Shannon entropies in low-dimensional quantum systems

Grégoire Misguich

Mémoire d'**habilitation à diriger des recherches** de l'Université Pierre et Marie Curie

Grégoire Misguich

Institut de Physique Théorique,
CEA Saclay
91191 Gif-sur-Yvette Cedex, France

Entanglement and Shannon entropies in low-dimensional quantum systems

Habilitation soutenue le 20 juin 2014 devant le jury composé de:

Benoît Douçot (Université P. et M. Curie, Paris)	Examinateur
Thierry Jolicœur (Université Paris-Sud, Orsay)	Examinateur
Andreas Läuchli (Innsbruck University)	Rapporteur
Philippe Lecheminant (Université de Cergy-Pontoise)	Rapporteur
Pierre Pujol (Université P. Sabatier, Toulouse)	Rapporteur
Tommaso Roscilde (École Normale Supérieure de Lyon)	Examinateur

17 octobre 2014, version 1.12

Contents

Résumé (français)

La première partie de ce mémoire traite de l'intrication quantique (entropie de Von Neumann) dans certains systèmes bidimensionnels. Il s'agit de fonctions d'onde de type Rokhsar-Kivelson (RK), construites à partir des poids de Boltzmann d'un modèle classique (modèle de dimères, de vertex ou de spins d'Ising par exemple). Nous montrons comment le spectre des matrices densité réduites de ces états s'obtient à partir des probabilités du modèle classique sous-jacent. Cette observation permet de calculer numériquement l'entropie d'intrication dans de grands systèmes, et en particulier de tester la présence de constantes sous-dominantes universelles dans le cas d'un liquide (de dimères) topologique de type $\mathbb{Z}_2$ (construction de Kitaev-Preskill & Levin-Wen) et dans le cas d'une fonction d'onde critique (dimères sur réseaux bipartites).

Si le système est un cylindre infiniment long et que le sous-système considéré est un demi-cylindre infini, le spectre de la matrice densité réduite peut se calculer plus simplement encore, par matrice de transfert. L'entropie d'intrication entre les deux moitiés du système apparaît alors comme l'entropie de Shannon associée aux probabilités des différentes configurations des degrés de liberté qui se trouvent à la frontière (un cercle). Ceci nous conduit à considérer l'entropie de Shannon (et ses généralisations de type Rényi) d'une fonction d'onde à N corps en tant que telle – indépendamment de son lien éventuel avec l'intrication quantique d'un état RK en dimension supérieure. Nous étudions les contributions universelles de cette entropie dans trois cas: 1) les liquides de Tomonaga-Luttinger, cadre dans lequel nous établissons un lien entre l'entropie de Shannon-Rényi et des problèmes de théories conformes avec bords, et calculons exactement les termes universels de l'entropie en fonction du paramètre de Luttinger et de l'indice de Rényi; 2) la chaîne d'Ising critique en champ transverse, pour laquelle nos simulations numériques montrent la présence d'une transition de phase à n=1 (indice de Rényi), qui reste mal comprise théoriquement, et pour laquelle une approche par méthode des répliques semble inadaptée; et enfin 3) des systèmes bidimensionnels avec symétrie continue spontanément brisée, où nous expliquons par un argument de champ libre (et de tour d'états) la présence de termes en $\log(L)$ dans l'entropie, comme récemment observé par simulations Monte-Carlo quantique.

Introduction

Quantum entanglement has become a central subject of research in the field of quantum many-body physics, and several concepts related to quantum information theory have found useful applications in the study of condensed matter models, from spin systems to the quantum Hall effect. Exact results are however relatively scarce in dimension greater than one and the starting point of the series of works summarized in this manuscript [1, 2, 3, 4, 5, 6] is "can we find some interacting quantum systems where the entanglement properties of large spatial regions could be computed exactly ?".

Boundary law

An important discovery of the last 15 years is that the low-energy states of short-ranged Hamiltonians are much *less* entangled than a state picked at random in the Hilbert space, or than a highly excited eigenstate of the same Hamiltonian. This is known as the *boundary law* [7] and it states that, in dimension D, the entropy of a subsystem of linear size L generically scales like $\sim L^{D-1}$.[1] This is much smaller than an extensive thermal entropy ($\sim L^D$) or much smaller than the extensive entanglement entropy (EE) of high energy eigenstates. The boundary law is relatively intuitive for states with a finite correlation length. In that case we may assume that entanglement mostly comes from those correlations taking place between degrees of freedom sitting across the boundary of the subsystem, hence a scaling with the size of the boundary. But making this more rigorous turns out to be quite difficult.[2]

This law has shed light on the huge success (and limitations) of the density matrix renormalization group (DMRG) method for one-dimensional systems [10, 11]. The modern view is indeed that DMRG is a variational approach in the space of matrix-product states, and that the amount of entanglement is the parameter which dictates how large the matrices should be in order to faithfully represent the actual wave function. Realizing this has also helped to apply the DMRG to 2D problems [12]. But understanding that a good Ansatz should (at least) be able to reproduce a boundary law has also opened the way to promising methods to treat interacting systems in higher dimensions: Projected entangled pair states (PEPS) [13], Tree tensor networks [14] or the Multiscale Entanglement Ansatz [15] to name a few.

Corrections to the boundary law

There are few examples of systems which ground state entropy exceeds the boundary law, but a very famous one is certainly the $\frac{c}{3}\log L$ divergence of the EE of a segment of length L in a

[1] This was originally discussed for black holes as the "area" law, where the two-dimensional horizon plays the role of a boundary [8]. Here, and in condensed matter in general, the space dimension D is between 1 and 3 and the term *boundary* law seems more appropriate than *area* for this L^{D-1} scaling.

[2] See for instance [9] for a proof in gapped 1D systems.

(much longer) critical chain with central charge c [16, 17, 18], which is a remarkable bridge between conformal field theory (CFT), quantum information and lattice many-body systems. Systems with a Fermi surface are another example [19].[3] Most other systems in dimension $D = 2$ do not violate the boundary law (the leading term is L^{D-1}) but they can have some universal subleading corrections, which may be $\mathcal{O}(\log L)$ in some geometries [20]. This manuscript presents some concrete examples and several exact results concerning logarithmic terms in critical states (so-called Rokhsar-Kivelson states).

The entanglement is also a useful way to probe gapped systems with short-range correlations. This is particularly true for topological phases of matter, where quantum information ideas have lead to some important advances. These phases cannot be characterized by any conventional local order parameter (they do not necessarily break any symmetry). They are nevertheless distinct from "conventional" phases, in the sense that a system cannot evolve continuously from a topological phase to a non-topological one without crossing a phase transition. The most famous examples of topological phases (or topological *order*) are those of the fractional quantum Hall effect (FQHE) [21] and gapped spin liquids (for reviews on the later, see for instance [22, 23, 24]). The study of quantum entanglement has allowed to define some precise ways to distinguish topological phases from non-topological ones, and also to distinguish different types of topological states. Kitaev and Preskill [25] and Levin and Wen [26] (see also [27, 28]) explained how to detect topological order from the ground state wave function alone, using a subleading correction to the EE of a (large) subsystem. This entropy constant is called the topological entanglement entropy (TEE), and will be illustrated with a simple example in Sec. 1.1. Their approach allows to obtain the *total quantum dimension* of the phase, which is a universal number related to the fractional quasi-particle content of the phase.[4] Previously, deciding if a given system has some topological order would have required to look at excited states wave functions, or to analyze how the ground state degeneracy changes when the topology is changed. But with EE as a diagnostic, topological order appears to be a property of the ground state alone. Furthermore, it was recently realized that studying entanglement can give access to more informations about the system, namely the braiding and statistics of the topological/fractional excitations [29].

But measuring the EE also became a *practical* and powerful tool to detect topological phases in numerical simulations. The EE can be measured using quantum Monte Carlo (QMC), as in [30] where a $\mathbb{Z}_2$ liquid phase was identified thanks to the TEE. For two-dimensional (2D) models with a sign problem, the DMRG has recently proved to be extremely useful, in particular because it gives access to the entanglement properties in long cylinder geometries. For instance, Refs. [31, 32, 33] used DMRG and entanglement analysis to propose some $\mathbb{Z}_2$ phases in several frustrated Heisenberg models, including the (nearest-neighbor) Heisenberg antiferromagnet on the kagome lattice. Some topological phase was also proposed for a particular magnetization plateau in the kagome Heisenberg antiferromagnet [34].

Entanglement spectrum

It was also realized that the *spectrum* of the reduced density matrix (RDM) of a large subsystem can be used to extract some information about the long-distance physics. In a seminal paper, Li and Haldane [35] showed that the entanglement spectrum (ES) of a quantum Hall

[3] A Fermi surface leads to an EE which scales as $\log(L)L^{D-1}$. This multiplicative $\log L$ correction can be though as arising from multiple 1D-like gapless modes located at each point of the Fermi surface.

[4] A definition is given in Sec. 1.3.2.

system *without any boundary* (on a sphere for instance) contains some information about the energy spectrum of the chiral gapless edge modes which can propagate if the system has a boundary (see also [25, 36]).

This remarkable "bulk-edge" correspondence has since then been tested (and sometimes understood) in many other systems, and lattice spin or boson models in particular. It would be impossible to cite here all the numerous works related to the study of ES. But we can list here a few examples in order to illustrate the great variety of problems which can studied using this new tool called "entanglement spectroscopy": Topological order in Haldane phase (spin-1 chains) and degeneracies in the ES [37]; relation between ES and edge modes in topological insulators and superconductors [38]; Entanglement between coupled spin-$\frac{1}{2}$ chains (ladder) [39, 40]; FQHE on spheres and entanglement gap [41]; FQHE on a torus and edge modes [42]; Critical spin chains and CFT operators [43, 44]; Tower of states in the ES of systems with gapless Nambu-Goldstone modes [45, 46]; Identification of a 2D chiral spin liquid in kagome-lattice antiferromagnet using DMRG and ES analysis [47]; $\cdots$

Quantum field theory

We have given several examples showing that the EE is a powerful tool to probe condensed-matter systems, in particular when doing numerical simulations. But these EE concepts are also of growing importance in quantum field theory (QFT). For instance, the EE has been found to play an important role in the anti-de Sitter(AdS)/CFT correspondence.[5] As a second example, closer to the present work, people have considered the EE $S(R)$ of the area enclosed in a disk of radius R in a 2+1D QFT. $S(R)$ is related to the free energy of a sphere in 3D and is of the form $S(R) = \alpha R - \gamma$, where γ is a (finite and universal) constant term. This γ has been shown to be somewhat analogous to the central charge in 1+1D CFT since it *decreases along RG trajectories* [49]. This "f theorem", which is based on Lorentz invariance and strong sub-additivity of the EE,[6] can therefore be used to exclude some particular RG flows. In other words, if some perturbation triggers an instability in a system described by a first fixed point, it can only flow to a second fixed point with *lower* γ. This "entanglement monotonicity" was in turn recently exploited to bring new results about the stability of some – much debated – gapless spin liquids[7] in the field of frustrated quantum magnets [52]. This is an example where QFT results have found some application in a strongly interacting fermion problem, via a quantum information concept.

Outline

The models we discuss in this manuscript are certainly simpler than the strongly interacting gauge theories involved in the spin liquids mentioned just above, but a large part of the present work aims at understanding and computing similar universal entropy constants. The first chapter explains how to calculate the EE and ES for a particular class of states in 2+1D, the so-called Rokhsar-Kivelson (RK) states. These states are obtained by "promoting" a classical lattice model (2+0D) to a wave function. They allow to import some knowledge

[5] The EE of a region in some (D+1)-dimensional CFT was conjectured to be proportional to the area of a minimal surface in a higher-dimensional curved (AdS) space [48].

[6] $S(A \cup B) + S(A \cap B) \leq S(A) + S(B)$.

[7] These spin liquids are described by Dirac fermions (spinons) interacting via a $U(1)$ gauge force [50, 51].

from 2D classical statistical mechanics (exactly solvable models and/or CFT) to construct tractable quantum models.

Critical RK states correspond to fine-tuned multi-critical points [53] and are therefore not completely representative of generic critical points encountered in microscopic 2+1D systems,[8] but as we will see, they offer a useful and controlled framework to discuss universal corrections to the boundary law in 2D. Gapped RK states are more "generic" in the sense that they have most of the qualitative properties of quantum massive states, and they can be particularly interesting to describe phases with topological order. The simplest of these topological phases, namely $\mathbb{Z}_2$ liquids, is discussed in Sec. 1.3.

This study of the EE in RK states reveals that the entanglement between two spatial regions is "mediated" through some degrees of freedom forming a quantum chain located along the boundary of the two subsystems. A useful finding is that, in some appropriate geometries, the EE turns out to be the Shannon entropy of the ground state of that chain (Sec. 1.4), which is an important simplification since the explicit trace over the degrees of freedom of one subsystem, and the subsequent diagonalization of the RDM, can be bypassed.[9]

This leads us in Ch. 2 to consider the Shannon entropy (and Rényi generalizations)[10] of a given wave function as an interesting quantity on its own, independently from the fact that it may be related to an EE in some higher-dimensional RK system. The main message we convey here is that, although the Shannon entropy is a basis-dependent quantity,[11] it contains some universal subleading corrections (in the limit of large system size). In Sec. 2.1 we provide a rather complete theory of these corrections in the case of Tomonaga-Luttinger liquids. For these systems we relate the subleading entropy constants to known boundary entropies of the compactified boson CFT, and show that they give access to the boson compactification radius R (or, equivalently, the Luttinger parameter). For instance, the subleading term in the Shannon entropy is shown to be $\log(R) - \frac{1}{2}$. We also discuss a phase transition which takes place at some critical value n_c of the Rényi parameter. For the Ising chain in transverse field (Sec. 2.2), our understanding is less complete than for the free boson, and still mostly based on numerical observations. In this system the critical value of the Rényi parameter is $n_c = 1$ and, although we could determine the universal entropy constant precisely at this point (Eq. 2.27), its understanding in term of field theory is still a challenge, in particular because a replica approach is not applicable.

The chapter 3 deals with systems with a spontaneously broken continuous symmetry and gapless Nambu-Goldstone modes. Using a free-field description we show that, in this case, the Shannon-Rényi entropy (SRE) of the ground state contains some corrections to the volume law which are logarithms of the system size, and the coefficient of these $\log(L)$ terms is proportional to the number of gapless modes. We compare our findings with some recent QMC results [54]. Contrary to the first two chapters, this last part mostly presents some unpublished results.

[8] Their critical exponents are those of a 2D field theory, and not 3D as one expects for a quantum system in two spatial dimensions.

[9] This construction does not only give the EE, but also the ES: the eigenvalues of the reduced density matrix are classical probabilities for the boundary degrees of freedom.

[10] For a definition of these entropies, see Eq. 2.1.

[11] The EE of the RK state is of course basis independent, but the RK wave function has a simple expression in terms of classical weights only in one particular basis, the one corresponding to the configurations of the underlying classical model. It is in this basis that the Shannon entropy of the boundary chain is equal to the EE of the RK state.

Chapter 1

Entanglement in Rokhsar-Kivelson wave functions

Calculating exactly the entanglement entropy of a large subsystem in a many-problem is usually quite difficult since it involves several tasks which scale exponentially with the system size. First, one has to get some description of the wave function, in some exponentially large Hilbert space. Then, one needs to trace over some part of the system, which also corresponds to an exponentially long calculation. One should finally diagonalize the RDM and sum over its eigenvalues.

The situations where the system maps onto free particles – fermions or bosons – is a notable exception since the RDM of a subsystem is Gaussian[1] and thus completely determined by the data of the one-body correlations inside the subsystem (Wick's theorem). In that case the entanglement entropy can be computed numerically in polynomial time, and analytically in many interesting cases [55, 56]. In the following sections we show how these tasks also greatly simplify for Rokhsar-Kivelson (RK) states.

1.1 Rokhsar Kivelson construction

In 1988 Rokhsar and Kivelson [57] introduced the first quantum dimer model (QDM). The historical motivation was to provide a simple model describing the physics of short-range resonating valence-bond (RVB) states, in relation to the physics of the cuprate superconductors.

In a QDM the Hilbert space is spanned by an orthonormal basis $\{|c\rangle\}$, where each basis state $|c\rangle$ is associated with an hard-core dimer covering of the lattice (see example in Fig. 1.1). The original RK model has the following Hamiltonian:

$$\mathcal{H} = \sum_{\text{Plaquette}} \left[-t \left(\left| \square \right\rangle \left\langle \square \right| + \text{H.c.} \right) + v \left(\left| \square \right\rangle \left\langle \square \right| + \left| \square \right\rangle \left\langle \square \right| \right) \right] . \tag{1.1}$$

The "kinetic" term (amplitude $-t$) flips two dimers around a square plaquette while the "potential" term (proportional to v) is diagonal in the dimer configuration basis and favors or penalizes plaquettes with two dimers ("flippable" plaquettes). The zero-temperature phase diagram of this model has been intensively studied [57, 58, 59, 60] and displays several crystalline phases with spontaneously broken translation symmetry. Here we focus on one

[1] It is the exponential of a quadratic form in the creation and annihilation operators.

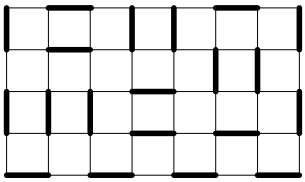

Figure 1.1: Hard-core dimer covering of the square lattice.

particular point (so-called *RK point*), where $t = v = 1$. There the Hamiltonian can rewritten as a sum of projectors

$$\mathcal{H}_{\mathrm{RK}} = 2\sum_p |\Psi_p\rangle \langle\Psi_p| \tag{1.2}$$

$$|\Psi_p\rangle = \frac{1}{\sqrt{2}} \left(\left| \begin{smallmatrix} \bullet & \bullet \\ \bullet & \bullet \end{smallmatrix} \right\rangle - \left| \begin{smallmatrix} \bullet & \bullet \\ \bullet & \bullet \end{smallmatrix} \right\rangle \right). \tag{1.3}$$

The linear superposition of all dimer coverings belonging to a given sector[2] Ω

$$|\mathrm{RK}_\Omega\rangle \sim \sum_{c\in\Omega} |c\rangle \tag{1.4}$$

is annihilated by Eq. 1.2 and is therefore a ground state.[3] This point lies between two crystalline phases for $v < 1$ and $v > 1$. The nature of the ground state for v slightly smaller than 1 is a subtle issue, but a resonating plaquette phase seems plausible [60]. For $v > 1$ the "staggered" dimer configurations (non-flippable) are the exact ground states.

This construction of a 2D wave function from a 2D classical model can be generalized to an arbitrary classical system, where each c can be an Ising or vertex configuration for instance [61]. When the Boltzmann weights are not all equal, the resulting generalized RK wave function has amplitudes which are the square roots of the classical Boltzmann weights:

$$|\mathrm{RK}_\Omega\rangle = \frac{1}{\sqrt{\mathcal{Z}}} \sum_{c\in\Omega} \sqrt{e^{-E(c)}}\, |c\rangle\,, \tag{1.5}$$

where the normalization factor $\mathcal{Z}_\Omega = \sum_{c\in\Omega} e^{-E(c)}$ is the classical partition function. Some Hamiltonians for which the state above is an exact ground state can easily be constructed [62, 61, 63]. These Hamiltonians can be chosen to be local as long as the classical energy $E(c)$ only contains short-ranged interactions.

[2] All the dimer configurations which can be obtained from each other by a succession of two-dimer flips (kinetic term of the Hamiltonian) form an ergodicity sector. In the following we will sometimes omit to specify Ω explicitly.

[3] The argument is the following. Consider a plaquette p and a configuration $|c\rangle$. If $|c\rangle$ has one or no dimer at all on the edges of p we have $\langle\Psi_p|c\rangle = 0$. If two dimers are present, then there exists in the same sector Ω a second configuration $|c'\rangle$ which only differs from $|c\rangle$ by a two-dimer flip on p. In such a case the combination $|c\rangle + |c'\rangle$ is again orthogonal to $|\Psi_p\rangle$. This shows that $\mathcal{H}_{\mathrm{RK}}\,|0\rangle = 0$.

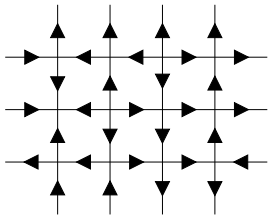

Figure 1.2: Example of 8-vertex configuration. The number of incoming arrow(s) is even (0,2 or 4) at each vertex.

1.2 Classically constrained models and RK reduced density matrix

We now describe the RDM of a RK state. The RDM ρ_A associated with a spatial region A is defined by tracing $\rho = |\mathrm{RK}\rangle \langle \mathrm{RK}|$ over the degrees of freedom living outside A:

$$\rho_A = \mathrm{Tr}_B \left[|\mathrm{RK}\rangle \langle \mathrm{RK}| \right]. \tag{1.6}$$

The structure of ρ_A is particularly simple for constrained models such as dimer models or vertex models.[4] This was, to our knowledge, first discussed in 2007 in the context of a QDM on the triangular lattice [1].

To illustrate this important idea we focus on a classical system where the allowed configurations are those of an 8-vertex model on the square lattice, that is with an even number of incoming arrows at each vertex (Fig. 1.2). Switching off some weights, this also includes the 6-vertex models. One can also represent an hard-core dimer problem if we change the parity constrain to "odd".[5]

1.2.1 Schmidt decomposition of a RK state

To compute the von Neumann entropy we need to diagonalize the reduced density matrix ρ_A. A practical way to do so is to find a Schmidt decomposition of the wave function. It amounts to write the state $|\psi\rangle$ as a sum of tensor-product states $\left|\psi_i^A\right\rangle \otimes \left|\psi_i^B\right\rangle$, where each $\left|\psi_i^A\right\rangle$ is a state of the region A, and each $\left|\psi_i^B\right\rangle$ is a state of the region B:

$$|\psi\rangle = \sum_i \sqrt{p_i} \left|\psi_i^A\right\rangle \otimes \left|\psi_i^B\right\rangle, \tag{1.7}$$

with the following orthogonality constrains:

$$\left\langle \psi_i^A \middle| \psi_j^A \right\rangle = \left\langle \psi_i^B \middle| \psi_j^B \right\rangle = \delta_{ij}. \tag{1.8}$$

The $\sqrt{p_i}$ are called the Schmidt eigenvalues, and since ρ_A can be written as

$$\rho_A = \sum_i p_i \left|\psi_i^A\right\rangle \left\langle \psi_i^A \right|, \tag{1.9}$$

[4] As discussed in Ref. [2], one can recover a simple density matrix structure for RK wave functions without hard-core constrains provided one artificially *duplicates* the degrees of freedom sitting at the boundary between the two subsystems, so that one copy is in A, and the other in B.

[5] Using the fact that the lattice is bipartite, an arrow going *out* of a vertex in sublattice A is a dimer, while an arrow going *in* sublattice A is an empty bond.

the $p_i \geq 0$ are the eigenvalues of ρ_A. The Eq. 1.7 makes apparent the fact the EE $S_1 = -\sum_i p_i \log p_i$ measures how "far" the state $|\psi\rangle$ is from a product state (which would correspond to a single non-zero eigenvalue $p_0 = 1$ and $S_1 = 0$). The Schmidt decomposition also shows that the EE measures how much information is gained on system A if one observes (projection) the region B to be in one of the states $\left|\psi_i^B\right\rangle$.

In a vertex model it is natural to define the subsystem A as a set of bonds, and B its complement. A bond $b \in B$ is said to belong to the *boundary* ∂B of B if it touches at least one bond in A (Fig. 1.3). The configurations of the boundary arrows, noted i or $|i\rangle$, will turn out to play an important role since they will label the eigenvalues of ρ_A. To see this we first note that a vertex configuration $|c\rangle$ can be decomposed as some part $|a\rangle$ sitting in region A, and some part $|b\rangle$ in region B (including its boundary):

$$|c\rangle = |a\rangle \otimes |b\rangle \tag{1.10}$$

Because the energy $E(c)$ of a given configuration c is a sum of vertex terms, it can be decomposed as follows:

$$E(c) = E^A(a,i) + E^B(b,i) \tag{1.11}$$

where a, b, c and i refer to the spatial decomposition introduced above. E^A is the total energy of the *vertices* which touch bonds of A and ∂B only, while E^B is the total energy of the vertices which only touch bonds of B (and also possibly in $\partial B \in B$).

The RK state can then be written as

$$|\mathrm{RK}\rangle = \frac{1}{\sqrt{\mathcal{Z}}} \sum_c |c\rangle \tag{1.12}$$

$$= \frac{1}{\sqrt{\mathcal{Z}}} \sum_{i \in \partial B} \left[\left(\sum_{a \in \Omega^A(i)} \sqrt{e^{-E^A(a,i)}}\, |a\rangle \right) \otimes \left(\sum_{b \in \Omega^B(i)} \sqrt{e^{-E^B(b,i)}}\, |b\rangle \right) \right] \tag{1.13}$$

where the first sum runs over all the configurations $|i\rangle$ of the boundary, and the two other sums run over the configurations of A and B which are compatible (parity constraint at each vertex) with the boundary configuration $|i\rangle$. The crucial point is that, for a given boundary configuration $|i\rangle$, the two sums over a and b are independent from each other. In other words, fixing i completely decouples the region A from the region B.[6] We also note that for some particular i, $\Omega^A(i)$ or $\Omega^B(i)$ may be empty.[7] The Eq. 1.13 can be re-written as:

$$|\mathrm{RK}\rangle = \sum_{i \in \partial B} \sqrt{p_i} \left|\mathrm{RK}_i^A\right\rangle \left|\mathrm{RK}_i^B\right\rangle \tag{1.14}$$

where $\left|\mathrm{RK}_i^A\right\rangle$ and $\left|\mathrm{RK}_i^B\right\rangle$ are some normalized RK states for subsystems A and B with a

[6] This is often referred to as a Markov property. PEPS states [13] — a larger class of Ansatz wave functions to which RK states belong — enjoy a similar Markov property: if one fixes the values of the *internal* tensor indices crossing the boundary between A and B, the two regions A and B get decoupled. This property implies a boundary law for the EE. Classical models with short-range interactions obviously have this property too. On the other hand, a generic quantum state does not have this property, even if it is the ground state of some Hamiltonian with short-ranged interaction and if it obeys the boundary law for the EE.

[7] This is the case if i forces the total number of incoming arrows in A to have the wrong parity.

fixed boundary i:

$$\left|\mathrm{RK}_i^A\right\rangle = \frac{1}{\sqrt{\mathcal{Z}^A(i)}} \sum_{a\in\Omega^A(i)} \sqrt{e^{-E^A(a,i)}}\,|a\rangle \tag{1.15}$$

$$\left|\mathrm{RK}_i^B\right\rangle = \frac{1}{\sqrt{\mathcal{Z}^B(i)}} \sum_{b\in\Omega^B(i)} \sqrt{e^{-E^B(b,i)}}\,|b\rangle\,. \tag{1.16}$$

The normalization factors are the classical partition functions of regions A and B with fixed i:

$$\mathcal{Z}^A(i) = \sum_{a\in\Omega^A(i)} e^{-E^A(a,i)} \text{ and } \mathcal{Z}^B(i) = \sum_{b\in\Omega^B(i)} e^{-E^B(b,i)}. \tag{1.17}$$

The p_i are classical probabilities to observe a given configuration i at the boundary:

$$p_i = \frac{\mathcal{Z}^A(i)\mathcal{Z}^B(i)}{\mathcal{Z}}. \tag{1.18}$$

The Eq. 1.14 looks like a Schmidt decomposition associated with the $A-B$ partition. To show that it is actually a Schmidt decomposition, we have to check the orthogonality conditions:

$$\left\langle \mathrm{RK}_i^A\right|\left.\mathrm{RK}_j^A\right\rangle = \delta_{ij} = \left\langle \mathrm{RK}_i^B\right|\left.\mathrm{RK}_j^B\right\rangle. \tag{1.19}$$

To show the above relations, it is enough to show that no configuration $|a\rangle$ in A can be simultaneously compatible with two distinct boundary configurations i and j.[8] Let us consider two configurations $|c\rangle = |ab\rangle$ and $|c'\rangle = |ab'\rangle$ which are identical inside region A. We will show that these two configurations must also have the same boundary configuration (with some caveat at the corners, see below).

We may compare graphically the two vertex configurations by coloring a bond if the arrows have different orientations in c and c', and leave it blank otherwise (Fig. 1.3, in green). Due to the parity constraint, this "transition graph" forms a set of (possibly intersecting) closed loops. None of these loops can touch a bond in A since, by definition, $|c\rangle$ and $|c'\rangle$ are identical in region A. It is easy to see that such loops cannot touch the boundary bonds without flipping some bonds inside A if the boundary is straight. So, in this case, two different boundary configurations necessarily lead to two distinct configurations in A (and also in B) and the orthogonality condition of the Schmidt vectors is verified. Some additional care is needed to define the boundary configurations when the region A has some corners.[9]

[8] Since the boundary region ∂B is included in B, it is obvious that if $i \neq j$ we have $\langle \mathrm{RK}_i^B|\mathrm{RK}_j^B\rangle = 0$ since both states have no common configuration (they at least differ along ∂B).

[9] The transition graph may flip pairs of boundary arrows at the "corners" of region A, without touching any arrow inside A. An example is shown in the lower right of Fig. 1.3 and it would contradict the Eq. 1.19. To deal with these situations, the two *corner* arrows should be merged into a single *boundary parity* $\sigma = \pm 1$. We choose $\sigma = -1$ if the two corner arrows point in different directions (one in and one out of A), and $\sigma = 1$ if the two corner arrows point in the same direction. With this convention, flipping the two corner arrows do not change σ, but flipping a single corner arrow does flip σ. With this construction, the boundary configuration i is made of the boundary arrows of the straight segments plus one parity σ for each corner. In the case where the boundary of A is a straight line, the boundary configurations are simply the arrow configurations of the blue bonds in Fig. 1.3a. This construction of the boundary degrees of freedom can be repeated for any A/B partition and it insures that Eq. 1.19 holds. The idea is that a boundary configuration i should contain, for each vertex in A which touches some bonds belonging to B, the parity of the number of arrows coming from region B. The analog construction for hard-core dimer models (on an arbitrary lattice) was discussed in Ref. [1].

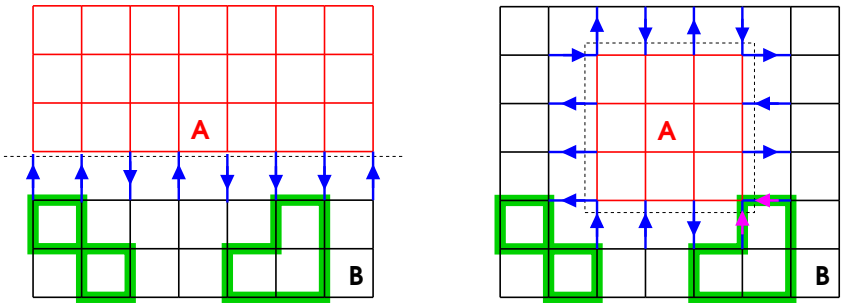

Figure 1.3: Spatial decomposition between regions A (bonds in red) and B (bonds in black or blue). The blue bonds correspond to the boundary ∂B. Green bonds: transition graph between two configurations which are identical in region A. Left: the boundary is straight and the transition graph cannot touch the boundary without also touching region A. Right: Case where region A has some corners. In the latter case the transition graph may flip a pair of adjacent boundary arrows (in magenta) in the corner, without flipping any bond in A. These two arrows should be combined into a single parity to represent a proper boundary degree of freedom (see text in footnote).

In the basis of the microscopic configurations, ρ_A is given by:

$$\langle a|\,\rho_A\,|a'\rangle = \begin{cases} \frac{p_i}{\mathcal{Z}^A(i)} \exp\left[-\frac{1}{2}\left(E^A(a,i)+E^A(a',i)\right)\right] & \text{if } a \text{ and } a' \text{ match bound. conf. } i \\ 0 & \text{otherwise} \end{cases} . \tag{1.20}$$

We thus see that, in this basis, ρ_A is made of blocks which are indexed by the boundary configurations.[10] Note that the RDM is properly normalized ($\mathrm{Tr}\,[\rho_A] = 1$) since $\mathcal{Z}^A(i) = \sum_a e^{-E^A(a,i)}$ and $\sum_i p_i = 1$. It is instructing to compare ρ_A with the thermal density matrix of the same subsystem in the *classical* model: the later is simply the diagonal of ρ_A. As we will see in Sec. 1.2.3, these two matrices have very different ranks, and different entropy scaling.

1.2.2 Spectrum of the RDM, von Neumann and Rényi entropies

We can read the spectrum of the RDM ρ_A from its Schmidt decomposition (Eq. 1.14): the (non-zero) eigenvalues of ρ_A are the p_i, that is the classical probabilities to observe the different boundary configurations (constructed as discussed above). In turn, the von Neumann entropy of the subsystem A is the Shannon entropy associated with these probabilities:

$$S^A_{\mathrm{VN}} = -\sum_i p_i \log p_i. \tag{1.21}$$

It is also useful to consider the Rényi entropy

$$S^A_n = \frac{1}{1-n} \log\left[\sum_i p_i^n\right], \tag{1.22}$$

[10] In the special case where all the classical energies vanish, the matrix elements inside a given block are identical and equal to $\frac{p_i}{\mathcal{Z}^A(i)}$; and $\mathcal{Z}^A(i)$ is the size of the block.

which reduces to the von Neumann entropy when $n \to 1$. The eigenvalues p_i can be interpreted as classical probabilities, proportional to some Boltzmann weights $p_i \sim \exp(-\mathcal{E}_i)$ associated to some effective classical interaction energy $\mathcal{E}_i$ among the boundary degrees of freedom. In this classical point of view, the Rényi parameter n plays the role of an inverse temperature, $p_i^n \sim \exp(-n\mathcal{E}_i)$. This additional parameter allows to extract more information from the system as it can be used to probe the ES at different "energies". As will be discussed in Sec. 2, there are cases where a phase transition takes place at some critical value of n. The Rényi entropies for integer $n \geq 2$ are also easier to compute analytically since they involve traces $\mathrm{Tr}\,[\rho_A^n]$, which can be accessed through a replica method. For the same reason, the Rényi entropies for integer $n \geq 2$ are also easier to access through QMC simulations [64].[11]

In some exactly solvable models these probabilities can be computed for relatively large systems (and large boundary length). This is the case of the hard-core dimer models on planar graphs, thanks to Kasteleyn's mapping onto Pfaffians [65] (see also [66]). This possibility was in particular exploited in Refs. [1] and [2] to compute the von Neumann entropy of various dimer RK states and for various subsystem geometries (for the results, see Sec. 1.3). In Sec. 1.4 will show how these probabilities can be computed using a transfer matrix approach if the system is an infinitely long cylinder (with finite circumference) and if A is a half-infinite cylinder.

1.2.3 Rank of ρ_A and boundary law

The rank of ρ_A for a generic wave function can be as high as the dimension of the Hilbert space of A. But here, for a RK state, all the non-zero eigenvalues of ρ_A are indexed by the boundary configurations. The number of such boundary configurations is bounded by some exponential of the length of the boundary (assuming that the classical model has a finite number of states per site). This implies, in turn, that the EE of A is bounded by some constant times the length of its boundary. So, RK states obey the boundary law.[12] This is not a surprising property if the system is gapped, but it is more interesting for gapless/critical states. If the classical model is critical,[13] we then have an explicit example of quantum critical wave function[14] which nevertheless obeys the boundary law.

Before concluding this section on the general properties of entanglement in RK states, we mention two other families of wave functions where RDMs which are "rank deficient" can also be found: PEPS states in lattice models [13] and model states (Laughlin, Moore-Read, etc.) in the field of the FQHE [35].

[11] In a simulation of n non-interacting copies of the system, $\mathrm{Tr}\,[\rho_A^n]$ is equal to the expectation value a unitary operator (called SWAP_n) which cyclically shifts the spins of region A among the n replicas and is the identity for the spins in B [64].

[12] They in fact obey a more strict law: the rank of the RDM is exponential in the length of the boundary.

[13] It could, for instance, be the equal amplitude combinations of all square-lattice dimer coverings, or some 6-vertex model in the critical region of its phase diagram.

[14] The observables which are diagonal in the classical basis have, by construction, the same expectation values in the RK wave function and in the classical model. So, if some correlation function decays algebraically in the classical system, it is also algebraic in the quantum $|\mathrm{RK}\rangle$ state.

1.3 Dimer models in the Levin-Wen and Kitaev-Preskill geometries

This section presents results obtained with S. Furukawa [1] and J.-M. Stéphan [6] concerning the entanglement properties of some RK states built from dimer coverings on the triangular lattice. These states are simple realizations of topological liquids and we begin by a brief introduction to short-range RVB states and $\mathbb{Z}_2$ liquids.

1.3.1 $\mathbb{Z}_2$ liquid phase

From the first ideas of about resonating valence-bonds (RVB) [67, 68], a huge number of works have dealt with the possibility that a 2D quantum antiferromagnet at zero temperature could have a ground state *without any magnetic long range order*.[15] However, until 2000, there was probably no widely accepted example of a quantum spin liquid (QSL) phase in a short-range spin Hamiltonian with $SU(2)$ symmetry.[16] In fact, at that time it was even not absolutely clear that such liquid states could exist *in principle*. In particular, the square lattice QDM of RK, which was somehow designed to describe a short-range RVB phase, failed to present any liquid phase.[17]

The QDM studied by Moessner and Sondhi in 2001 [74] is the triangular-lattice version of the model by Rokhsar and Kivelson:

$\mathcal{H} =$ $-t$ $\sum_r$ ($|$  $\rangle\langle$  $|$ + H.c.)

$+v$ $\sum_r$ ($|$  $\rangle\langle$  $|$ + $|$  $\rangle\langle$  $|$) , (1.23)

where the sum runs over all the rhombi r of the lattice. It is of course not a *spin* model, however, in the spirit of the overlap expansion [57], QDMs can be considered as effective (or phenomenological) descriptions of short-ranged RVB phases. So, the discovery that the triangular lattice QDM has a gapped liquid phase without any spontaneously broken symmetry was an important result.[18] It showed that such long sought short-range RVB phase could existed in simple models and revived the search for spin liquids in Heisenberg-like spin models.[19] But why are spin liquids interesting ? A possible answer is that they do not have

[15] There are some trivial examples of Heisenberg models without any broken symmetry: consider for instance an assembly of decoupled dimers. Such a system has a gap and all connected correlation functions are short-ranged. To exclude such states, which are not genuine Mott insulating phases but which are instead adiabatically connected to a band insulator, we may restrict ourselves to spin models with a *half-odd integer spin per unit cell*. This insures that there is no simple decoupled limit. For more precise definitions of quantum spin liquids, see for instance [24].

[16] There were however already several numerical studies which pointed to some "good candidates". Let us mention for instance the kagome Heisenberg antiferromagnet [69] or the ring-exchange model on the triangular lattice [70, 71]. Gapped spin liquids of $\mathbb{Z}_2$ type were also well understood using Schwinger boson mean-field theory [72, 73].

[17] The only point where the model does not order is a critical point.

[18] The initial estimate [74] of the extension of the liquid phase ($0.6 \lesssim v/t \leq 1$) has been refined ($0.825(25) \lesssim v/t \leq 1$) using extensive QMC simulations [75, 76, 77].

[19] A few years later, the discovery that the Herbertsmithite mineral was a spin-$\frac{1}{2}$ system with antiferromagnetic interactions, a kagome geometry, and no magnetic order at the lowest temperatures [78, 79] gave a huge boost the the field of QSLs. But all experiments so far point to a *gapless* liquid in this compound, so it is

any direct classical analogs and harbor exotic elementary excitations as well as some non-local entanglement. The later will be discussed in some details in the next section. To see that something interesting must be going on in QSL, we can invoke the Lieb-Schultz-Mattis theorem [82] and its higher dimensional generalization by Hastings [83] (see also [84, 85]). It guaranties that a Mott insulator is either gapless, or has some ground state degeneracy.[20] Usually, ground state degeneracies are the signature of some spontaneous symmetry breaking. As for gapless excitations, their most common origin in magnets is the Nambu-Goldtsone mechanism (typically spin waves). However, by definition, a QSL respect all lattice symmetries as well as the spin rotation symmetry. So, the degeneracy (or gaplessness) imposed by the Lieb-Schultz-Mattis-Hastings theorem cannot be understood from the conventional point of view. This is already a hint that QSL wave functions possess some interesting topological (or critical) properties. In the gapped cases (such as $\mathbb{Z}_2$ liquids), this is the notion of "topological order" introduced by Wen [86, 87] for spin systems and Wen and Niu [21] in the FQHE. This topological degeneracy is deeply related to the exotic nature of the elementary excitations in a QSL [88].[21]

1.3.2 Topological entanglement entropy

Subleading entropy constant

Levin and Wen (LW) [26] and Kitaev and Preskill (KP) [25] found a way to extract some information about the presence of topological order from the scaling of the EE. The idea is to look for corrections to the boundary law in the EE:

$$S \simeq \alpha L - \gamma + o(1) \tag{1.24}$$

where the first term represents the boundary law for a subsystem of linear size L and γ is the subleading constant of interest. Let us assume that correlation functions are short-ranged, with a correlation length ξ.[22] The simplest source of entanglement between the region A and its complement are the correlations between degrees of freedom inside A and outside A, and those are significant only if they are located at a distance smaller than ξ. So, these correlations are expected to contribute to the EE by an amount proportional to the number of degrees of freedom sitting in a shell of width ξ around the boundary. This corresponds to the boundary law. With this picture, it appears possible that local correlations would not contribute to the constant γ. In other words, perturbing the wave function by modifying its short distance correlations should change the boundary-law coefficient α but it should not affect γ. We thus expect γ to be only sensitive to some long-distance properties of the system and this quantity is a good candidate to represent some universal data about the phase.

presumably not of the simpler $\mathbb{Z}_2$ type we describe here. Among other experimental realizations of QSL in 2D, also gapless, we can mention some organic salts [80] and atomic monolayers of He^3 adsorbed on graphite [81].

[20] It applies to spin Hamiltonians which i) are translation invariant in one direction (say x), ii) have an odd number of half-odd-integer spins in the transverse direction (2D case), iii) a conserved magnetization $S^z_{\rm tot} = \sum_i S^z_i$, and iv) short-ranged interactions.

[21] QSL have "spinons" excitations which carry a spin $\frac{1}{2}$ (like an electron) but no electric charge. $\mathbb{Z}_2$ QSL also have Ising vortices excitations (dubbed visons) which are non magnetic and have a nontrivial mutual statistics with the spinons. The bound states of a vison and a spinon have a fermionic mutual statistics.

[22] One way to define ξ independently of any particular choice of correlator would be to analyze the correlation density matrix [89] or the mutual information [90].

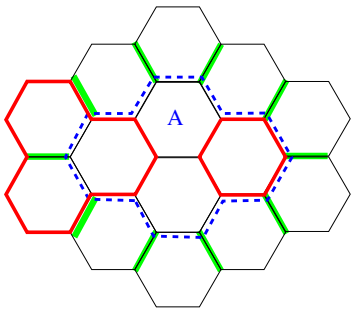

Figure 1.4: Loop configuration on the hexagonal lattice. The closed loops are in red, and the subsystem is the region A (set of bonds) enclosed by the dashed blue line. A boundary configuration lives on the green bonds. The number of loop strands crossing the boundary of A must be even and this non-local constrain is at the origin of the $-\log 2$ term in the EE.

Quantum dimension

LW explicitly computed γ for a series of gapped exactly solvable models with topological order (string-net models [91]) and showed that

$$\gamma = \log \mathcal{D}, \tag{1.25}$$

where $\mathcal{D}$ is the total quantum dimension of the phase.[23]

To gain some intuition about the origin of this term, it is instructing to start with the simplest string-net state, with $\mathbb{Z}_2$ topological order (as in [26]). It is a quantum superposition of closed and non-intersecting loop configurations on the honeycomb lattice. In a loop configuration each bond of the lattice can be occupied by a loop strand, or empty. The constrain is that each site touches zero or 2 strands (Fig. 1.4). The wave function is then the equal-amplitude superposition of all possible loop configurations. This state has a vanishing correlation length because two bonds which do not touch a common site can be shown to be uncorrelated.[24] Now consider a region A which has the topology of a disk. Since this state has the form of a constrained RK state, the EE of region A can be computed from the classical probabilities p_i of the boundary configurations, as in Sec. 1.2.1. In this loop model, a boundary configuration is defined by the positions where loop strands cross the boundary of A (green bonds in Fig. 1.4). For a boundary of length L, there is a maximum of 2^L boundary configurations. But only half of them can actually occur since the number of loop strands

[23] When k identical quasiparticles of type α are kept fixed an far apart, the Hilbert space dimension scales as $\dim(\alpha, k) \sim (d_\alpha)^k$ ($k \gg 1$) where d_α is called the *quantum dimension* of the α-particle. For topologically trivial excitations, we simply have a unique state whatever k and $d_\alpha = 1$. However, for non-Abelian fractional quasiparticles fixing their position may leave some degeneracy. While $\dim(\alpha, k)$ is necessarily an integer, the quantum dimension d_α need not be so. The total quantum dimension $\mathcal{D}$ of the phase is related to the individual quantum dimensions by $\mathcal{D} = \sqrt{\sum_{\alpha=1}^{N} d_\alpha^2}$, where N is the total number of topologically distinct types of quasiparticles. In a phase without any topological order there is a single type of (topologically trivial) quasiparticles with $d_0 = 1$, and therefore $\mathcal{D} = 1$. In the case of topological orders described by a *discrete* Abelian gauge theory (e.g., $\mathbb{Z}_n$), there are $N = n^2$ types of quasi-particles. They all have $d_\alpha = 1$ (Abelian) and $\mathcal{D}$ is equal to the number of elements in the gauge group.

[24] This state is exactly equivalent to a dimer liquid state of the kagome lattice [92] and closely related to Kitaev's toric code [25].

entering A must be even. One can further show that all the 2^{L-1} boundary configurations satisfying this parity constrain are equally probable, hence $p_i = 2^{1-L}$. We thus get an entropy $S_n^A = L\log 2 - \log 2$, where the $-\log 2$ reflects the topological order (and is independent from the Rényi index n). We thus see in this example that the TEE comes from a non-local constrain, which here simply originates from the fact that the bond degrees of freedom are constrained to form closed loops. This loop picture remains qualitatively correct for more complex $\mathbb{Z}_2$ states with a finite correlation length.

Deriving Eq. 1.25 for a general theory is not simple, but KP [25] also proposed a simple heuristic argument which can be summarized as follow. One first assumes that one can replace the reduced density matrix ρ_A by $\sim \exp(-\beta\mathcal{H})$, where $\mathcal{H}$ is the Hamiltonian of some 1+1D CFT describing a quantum system living on the boundary of A. This is certainly incorrect for the boundary law part, but it may capture the finite part. With this "nontrivial but natural" [25] assumption, the ground state EE of region A is the thermal entropy of the periodic 1D quantum system. The later is related to some standard torus partition function in CFT and can be shown to have a constant term $-\log\mathcal{D}$. Here $\mathcal{D}$ comes from the data of the modular S matrix of the CFT and is mathematically closely related to the Affleck-Ludwig entropies [93] (which will also appear in Sec. 2.1.2). We also note that, for a topological phase with gapless edge modes (FQHE for instance), this argument already contains/assumes the idea that the ES is related to the physics of the edge ($\mathcal{H}$).

Subtraction schemes

The Eq. 1.24 is really useful only if the two terms can be distinguished in practice, but separating the topological term $-\gamma$ from the boundary term in Eq. 1.24 is not completely obvious, in particular on a lattice. This is due to the fact that, on a lattice, the discrete nature of the boundary makes it difficult to define accurately the length L. This was illustrated in Ref. [1] at the RK point of the triangular lattice QDM. We considered subsystems composed of bonds lying inside a disk of increasing radius on a triangular lattice, and showed that the unavoidable ambiguity in the radius definition, although small, makes it impossible to extract γ directly.

KP and LW found indeed two ways to define γ by forming a linear combination of the EE on several subsystems. These subsystems share some common boundaries in such a way that the boundary terms cancel out from the combination, leaving the topological term γ. The proposed geometries differ in LW and KP schemes, but the idea is very similar.[25] In KP's work the topological constant is obtained from

$$S_{ABC} - (S_{AB} + S_{BC} + S_{CA}) + (S_A + S_B + S_C) \simeq -\gamma, \tag{1.26}$$

where the different subsystems A, B, etc. are shown in Fig. 1.5. It can easily be checked that all the local/boundary contributions cancel out since each segment of a boundary appears once with a plus sign and once with a minus sign in Eq. 1.26. Consider for instance the segment which separates A and B: it appears in the boundary of A and B (with + sign) as well as AC, BC (with − sign). The contributions from the corners also cancel out in a similar way. So, if the correlation length is sufficiently small compared to the dimensions of

[25] We note that, in KP's scheme, a conventional gapped phase with spontaneous discrete symmetry breaking would give a (negative) constant $\gamma = -\log(\text{deg})$ where deg is the ground state degeneracy. On the other hand, LW's scheme gives zero in such a case.

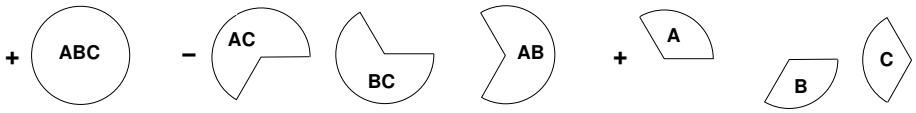

Figure 1.5: Kitaev-Preskill [25] scheme to extract the TEE. These seven different subsystems (built from three regions A, B and C) are those appearing in Eq. 1.26. A lattice version of the regions A, B and C is shown in Fig. 1.7

the various regions (disk radius), the entanglement which remains from the combination of Eq. 1.26 is not due to local correlations.

1.3.3 Numerical results in the liquid phase ($t \neq 0$)

We consider a family of generalized RK wave functions built from dimer coverings of an *anisotropic* triangular lattice. In the classical model the Boltzmann weight of a given dimer configuration c is $t^{n(c)}$, where $n(c)$ is the number of dimers sitting on the diagonal bonds (Fig. 1.6) and t the fugacity of these diagonal bonds (the other bonds have fugacity 1). The associated RK wave function is then

$$|\mathrm{RK}\rangle = \frac{1}{\sqrt{\mathcal{Z}}} \sum_c \left(\sqrt{t}\right)^{n(c)} |c\rangle \,, \tag{1.27}$$

where

$$\mathcal{Z} = \sum_c t^{n(c)} \tag{1.28}$$

is the classical partition function. For $t = 1$, $|\mathrm{RK}\rangle$ is simply the equal amplitude superposition of all coverings of the isotropic triangular lattice. This state is known to be a $\mathbf{Z}_2$ liquid state with topological order. This result was obtained by analyzing its (short-ranged) correlations and topological degeneracy [74, 94, 95, 96]. To our knowledge Ref. [1] was the first numerical measurement of the topological entanglement entropy using the method proposed by LW and KP,[26] and it confirmed the theoretical expectation – namely $\gamma = \log(2)$ – in a lattice model with a finite correlation length.[27] Since then a few other studies have used the LW and/or KP scheme to measure numerically γ in lattice models [98, 30].

The idea is to compute the probability p_i of each boundary configuration i (see Eq. 1.18) as the expectation value of some correlator in the classical dimer model.[28] If the whole system is finite, such a probability can be obtained by direct enumeration, as was done in [1]. If the boundary has a finite length but the subsystem A lives in a *infinite system*, one can still compute each p_i using a method based on Pfaffians. This was achieved in [6].

The different panels of Fig. 1.8 correspond to RK wave functions with different values of the parameter t, from the isotropic triangular lattice ($t = 1$) to the square lattice limit

[26] Just before, Haque *et al.* [97] did the first numerical estimation of TEE for a system in the continuum (Laughlin wave functions), but they did not implement the spatial partitioning proposed by LW and KP to extract the subleading constant.

[27] We specify here *finite* correlation length to contrast with some simpler wave functions like that of Kitaev's toric code [25] or the RK state for dimers on the kagome lattice [92] where all connected correlation functions are exactly zero beyond a few lattice spacings. In the later cases the constant γ can be obtained exactly.

[28] This correlator is 1 if the dimer at the boundary matches the boundary configuration i, and vanishes otherwise.

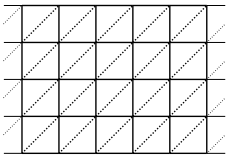

Figure 1.6: Triangular lattice with two different fugacities: the dashed diagonal bonds have fugacity t while the others, forming a square lattice, have fugacity 1.

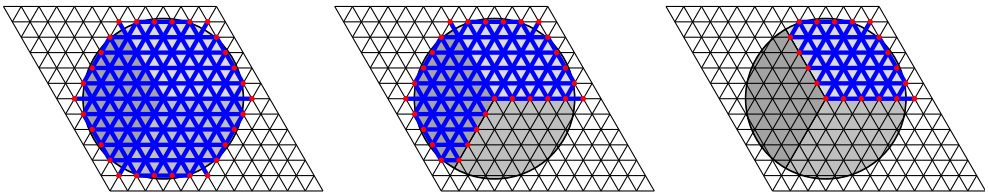

Figure 1.7: Geometries required for the computation of $S_n^{(\mathrm{ABC})}$, $S_n^{(\mathrm{AB})}$ and $S_n^{(\mathrm{A})}$ at Radius $\rho = 4.5$. They have $N_b = 30$, 29 and 19 boundary sites (in red) respectively. Taken from [6].

($t = 0$). The state is expected to remain in the gapped $\mathbb{Z}_2$ phase for all $t \neq 0$ and is critical only at $t = 0$, as can be checked using dimer-dimer correlations for instance [94]. We indeed observed that for $t = 0.3, 0.7$ and 1 the combination of Eq. 1.26 converges to $\gamma \simeq \log(2)$ when the radius of ρ of the subsystem ABC is increased (see Fig. 1.7 for an illustration at $\rho = 4.5$ lattice spacings). In fact, not only the von Neumann TEE converges to $\simeq \log(2)$, but also the other Rényi entropies we considered (from $n = 0.5$ to $n = 2$). The numerical data therefore confirms (in this $\mathbb{Z}_2$ case) the earlier prediction of Ref. [99] that the TEE is independent of the Rényi index. This confirmation is important for the practical use of the TEE to detect topological phases since the entropies which are most easily accessible in QMC simulations are those with integer $n \geq 2$. We finally note that the convergence is slower when t is small. This can be explained from the fact that the correlation length $\xi(t)$ diverges when $t \to 0$.

1.3.4 Critical point – square lattice ($t = 0$)

Finally we note in Fig. 1.8 that no clear limit can be extracted from the available radii at the critical point, and the question of the $\rho \to \infty$ limit remains an open problem (see also [20]). To simplify the discussion, let us focus on the $n \to \infty$ limit of the Rényi entropy $S_n = \frac{1}{1-n} \log\left(\mathrm{Tr}\rho_A^n\right)$, which selects the largest eigenvalue $p_{\max}$ of ρ_A (assumed to be non-degenerate):

$$S_\infty = -\log\left(p_{\max}\right). \tag{1.29}$$

Here $p_{\max}$ is the probability of the boundary configuration with the highest probability. To address the universal contributions to $p_{\max}$, we can go to the continuum limit of the problem. In the long distance limit the classical dimer model on the square lattice is described by a compactified Gaussian field. In the later theory the boundary configuration with the highest probability is that of a constant ("flat") value of the field along the boundary, that is a Dirichlet condition. So, the $p_{\max}$ of a given subsystem Ω is the ratio of the free field partition function $\mathcal{Z}_{D,\partial\Omega}$ with Dirichlet boundary condition along the boundary $\partial\Omega$, by the partition

function $\mathcal{Z}$ without any constraint:

$$p_{\max} = \frac{\mathcal{Z}_{D,\partial\Omega}}{\mathcal{Z}} \tag{1.30}$$

$$-\log(p_{\max}) = F_\Omega + F_{\bar{\Omega}} - F_{\Omega\cup\bar{\Omega}} \tag{1.31}$$

where the second line involves the free energies of Ω, its complement $\bar{\Omega}$, and the whole system (with Dirichlet boundary conditions).[29] Depending on the presence of sharp corners or non-zero Euler characteristics in Ω, $\bar{\Omega}$ and $\Omega\cup\bar{\Omega}$, these free energies may have some logarithmic part [100, 101]:

$$F_\Omega = aL^2 + bL + c\log(L)\left[\frac{\chi}{6} + \frac{1}{24\pi}\sum_i \gamma_i\left(1-\frac{\pi^2}{\gamma_i^2}\right)\right] + \mathcal{O}(1) \tag{1.32}$$

where the sum runs over the sharp angles γ_i of the boundary and c is the central charge of the CFT (here $c=1$ for a massless free field). For the geometries displayed in Fig. 1.7 (embedded in large disk for instance), all the area ($\sim L^2$) and linear ($\sim L$) parts cancel from Eq. 1.26. The topology of all the subsystems $\Omega = A, B, C, AB, \cdots$ is that of a disk and therefore $\chi_\Omega = 1$. The complement $\bar{\Omega}$ is an annulus ($\chi_{\bar{\Omega}} = 0$), and $\chi_{\Omega\cup\bar{\Omega}} = 1$. We therefore have, for each Ω, a cancellation of the logarithms coming from the Euler characteristics: $\chi_\Omega + \chi_{\bar{\Omega}} - \chi_{\Omega\cup\bar{\Omega}} = 0$. Finally one should consider the corner contributions. It is easy to check that in Eq. 1.26, each angle appearing in some $+S_\Omega$ cancels out with another one (with the same angle or its complement) in $-S_{\Omega'}$. However, as already mentioned in Ref. [30], this is only true for the leading (logarithmically divergent) part. Indeed, each $\log(L)$ is in fact $\log(L/a)$, with a some microscopic length scale. There is no simple reason why these microscopic scales should all be exactly the same in all the terms. We thus expect that Eq. 1.26 should give a non-universal (and therefore n dependent) constant term when $t=0$, which is compatible with our numerical results at $t=0$.

1.4 Long cylinder geometry

The previous section explained that the spectrum of a RDM for a RK state is given by the classical probabilities p_i of some boundary configurations of the system. There is one particular geometry where the calculation of these probabilities simplifies considerably: an infinitely long cylinder of finite circumference L, where the subsystem A is an semi-infinite cylinder (Fig. 1.9). As first discussed in [2], the probabilities are simply obtained in terms of the dominant eigenvector of the classical transfer matrix. This geometry is not only simpler for calculations in RK states, it is also particularly well suited to compute the TEE because, as we will see, it allows to extract γ without the need to implement the subtraction schemes of LW or KP.

1.4.1 Classical transfer matrix and p_i

We consider a classical model of the type discussed in Sec. 1.1, and we take the example of a vertex model on the square lattice for simplicity. We denote by $\mathcal{T}$ the transfer matrix

[29] In [20] this formula was used for the von Neumann entropy ($n=1$), which is not always justified (more details in Sec. 2.1.2).

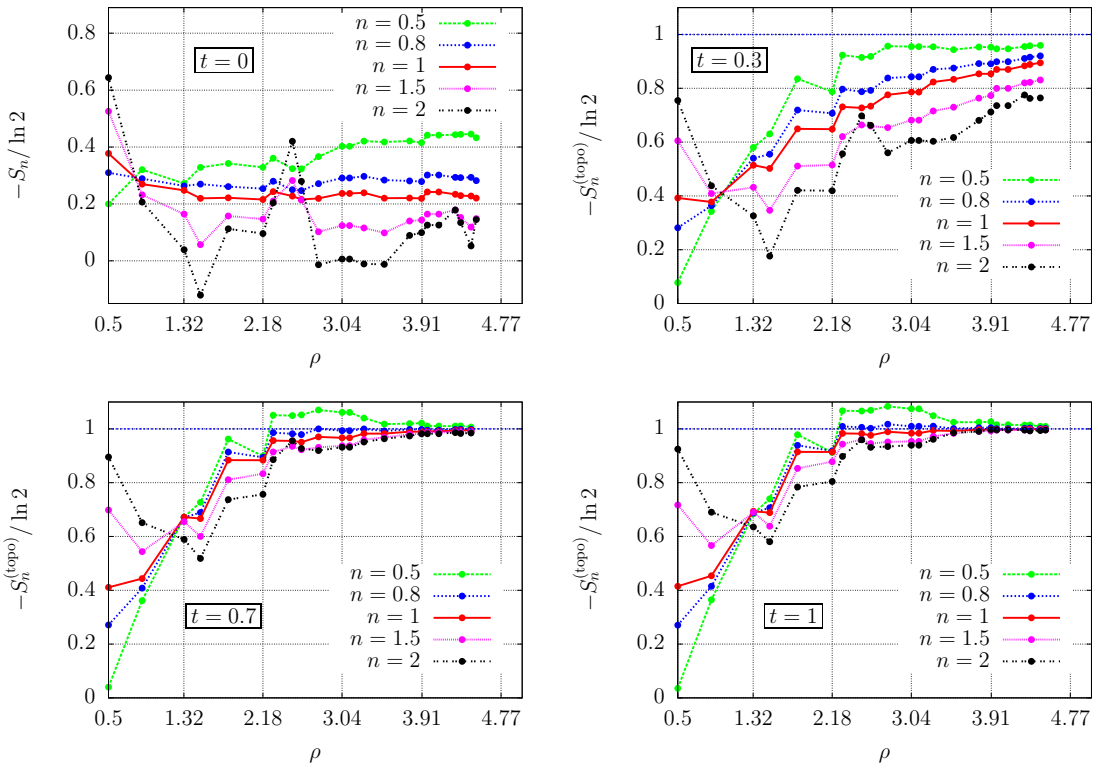

Figure 1.8: Topological entropy constant S_n^{topo} (same as $-\gamma$, Eq. 1.26) for various values of the Rényi index n, as a function of the disk radius ρ. Top left: critical case $t = 0$. Top right: $t = 0.3$. Bottom left $t = 0.7$. Bottom right $t = 1$. From [6].

which connects the arrow configurations of one line to the next line, as shown in Fig. 1.9. We assume that $\mathcal{T}$ is real symmetric to simplify slightly the notations (left and right eigenvectors are the same and the eigenvalues are real). If $|a\rangle$ and $|b\rangle$ represent the boundary conditions at both ends of the cylinder ($y = \pm l_y$) the probability p_i of a configuration $|i\rangle$ is:

$$p_i = \frac{\langle a| \mathcal{T}^{l_y} |i\rangle \langle i| \mathcal{T}^{l_y} |b\rangle}{\langle a| \mathcal{T}^{2l_y} |b\rangle}. \tag{1.33}$$

Now we take the $l_y \to \infty$ limit with L fixed, and assume that the eigenvector $|g\rangle$ corresponding the largest eigenvalue λ of $\mathcal{T}$ is non-degenerate and has a finite overlap with $|a\rangle$ and $|b\rangle$. In this limit we can approximate $\mathcal{T}^{l_y}$ by

$$\mathcal{T}^{l_y} \overset{l_y \gg L}{\simeq} \lambda^{l_y} |g\rangle \langle g| . \tag{1.34}$$

which gives:

$$p_i \overset{l_y \gg L}{\simeq} \frac{\lambda^{l_y + l_y} \langle a|\, g\rangle \langle g\, |i\rangle \langle i|\, g\rangle \langle g|\, b\rangle}{\lambda^{2l_y} \langle a|\, g\rangle \langle g\, |b\rangle} = |\langle g|\, i\rangle|^2 . \tag{1.35}$$

So, the eigenvector $|g\rangle$ contains the information about all the probabilities p_i, and therefore contains the ES of the half-infinite cylinder A. In particular, the explicit integration over the degrees of freedom in region B have been avoided. The task has been reduced to diagonalizing

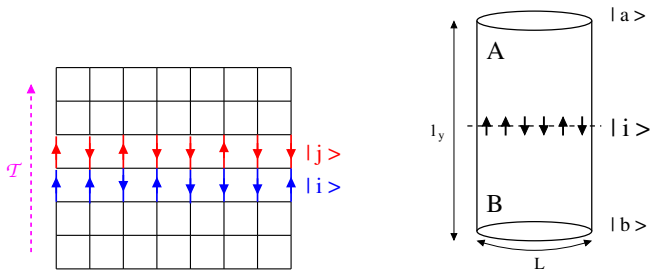

Figure 1.9: Left: Two boundary configurations of a vertex model $|i\rangle$ and $|j\rangle$ which are connected by a transfer matrix $\mathcal{T}$. Right: cylinder geometry, with subsystems A and B.

$\mathcal{T}$, which dimension is exponential in L, but independent of l_y. For a general model this can be done numerically.

1.4.2 Classical mutual information

Before going on with the entanglement in RK states we wish make a few remarks about its connection to classical mutual information. The mutual information is defined as:

$$I_n(A,B) = \frac{1}{2}\left(S_n^A + S_n^B - S_n^{AB}\right), \tag{1.36}$$

where $S_n^\Omega = \frac{1}{1-n}\mathrm{Tr}\left[\rho_\Omega^n\right]$ is the Rényi entropy of part Ω. It has recently received some attention in quantum [90, 102, 103, 104] and classical systems [105, 106, 107]. $I_n(A,B)$ reduces to the EE for pure states at $T=0$ since in that case $S_n^A = S_n^B$ and $S_n^{AB} = 0$. At finite temperature each entropy obeys a volume law (as thermodynamic entropies) but $I_n(A,B)$ will in general scale as the size of the boundary between A and B, and is the analog of EE for thermal states. This quantity is sensitive to "global" – *i.e.* independent of any choice of correlator– correlations between the two different regions, and is equally sensitive to quantum and classical correlations. It measures how much information is gained on part B when one observes the state of region A.

As we will see, the mutual information $I_n^{\mathrm{class}}(A,B)$ of a classical system is closely related to the EE of the associated RK state. We start from the same classical (constrained) model, but now in a classical thermal/Gibbs state. The entropy of region A is

$$S_n^{A\ \mathrm{class}} = \frac{1}{1-n}\log\left[\sum_{ia}\left(p_{ia}\right)^n\right], \tag{1.37}$$

where i labels the boundary configuration between region A and B, and a labels the "spins" inside region A (note the difference with Eq. 1.22). The probability p_{ia} can be written as

$$p_{ia} = p_i\frac{\exp\left(-E^A(a,i)\right)}{\mathcal{Z}_i^A} \tag{1.38}$$

$$p_i = \frac{\mathcal{Z}^A(i)\mathcal{Z}^B(i)}{\mathcal{Z}} \tag{1.39}$$

where $\mathcal{Z}^A(i)$ is the partition function of the region A with the fixed boundary configuration i (as in Eq. 1.17), and p_i is the probability of that configuration (as in Eq. 1.18). As for the RK

construction, the temperature is set to 1 (absorbed into the definition of the energy). Using these notations, the entropy of (say) A reads:

$$S_n^{A\ \text{class}} = \frac{1}{1-n}\log\left[\sum_i (p_i)^n \sum_a \left(\frac{\exp\left(-E^A(a,i)\right)}{\mathcal{Z}^A(i)}\right)^n\right] \tag{1.40}$$

$$= \frac{1}{1-n}\log\left[\sum_i \left(\frac{p_i}{\mathcal{Z}^A(i)}\right)^n \sum_a \exp\left(-nE^A(a,i)\right)\right] \tag{1.41}$$

$$= \frac{1}{1-n}\log\left[\sum_i \left(\frac{\mathcal{Z}^B(i)}{\mathcal{Z}}\right)^n \tilde{\mathcal{Z}}^A(i)\right] \tag{1.42}$$

where $\tilde{\mathcal{Z}}_i^A$ denotes that the partition function of the region A is evaluated at temperature $1/n$ (Boltzmann weight raised to the power n). As for the mutual information, Eq. 1.36 becomes:

$$I_n^{\text{class}}(A,B) = \frac{1}{2(1-n)}\log\left[\frac{\sum_i \left\{\left(\mathcal{Z}^B(i)\right)^n \tilde{\mathcal{Z}}^A(i)\right\}\sum_j \left\{\left(\mathcal{Z}^A(j)\right)^n \tilde{\mathcal{Z}}^B(j)\right\}}{\mathcal{Z}^n \sum_i \tilde{\mathcal{Z}}^A(i)\tilde{\mathcal{Z}}^B(i)}\right]. \tag{1.43}$$

At this point we may again adopt the infinitely long cylinder geometry, so that each of the partition functions above can be expressed using the dominant eigenvector $|g\rangle$ of the transfer matrix $\mathcal{T}$ (at temperature 1), and using the dominant eigenvector $|\tilde{g}\rangle$ of the transfer matrix $\tilde{\mathcal{T}}$ at temperature $1/n$. After a few simple manipulations, similar to those of Sec. 1.4.1, one gets

$$I_n^{\text{class}}(A,B) = \frac{1}{1-n}\log\left[\sum_i \langle\tilde{g}|\ i\rangle\ \langle i|\ g\rangle^n\right], \tag{1.44}$$

which only requires a summation over the boundary configurations.[30] If the classical energies are all zero, the two temperature 1 and $1/n$ are in fact equivalent and $|g\rangle = |\tilde{g}\rangle$. Due to the hard-core constrains the problem can nevertheless be non-trivial, as we know from the examples of dimer or vertex models. The classical mutual information above is then $I_n^{\text{class}}(A,B) = \frac{1}{1-n}\log\left[\sum_i (p_i)^{\frac{n+1}{2}}\right]$, which, up to a redefinition of n is identical to the *quantum* EE $S_{n'}^A = S_{n'}^B$ defined in Eq. 1.22, provided $n' = \frac{n+1}{2}$. This connection between classical mutual information and quantum EE of a RK state was obtained in Ref. [108], except that the (important) condition that the classical energies should vanish was apparently overlooked. When the classical energies do not vanish, the correct expression is Eq. 1.44.

1.4.3 A free fermion case

Let us go back to the EE of RK states. There are systems where $\mathcal{T}$ can be diagonalized by simple means. This is the case, for instance, of dimer models on the square or hexagonal lattices, where $\log\mathcal{T}$ is a simple free fermion Hamiltonian. It is also the case for one point of the 6-vertex model phase diagram (corresponding to $\Delta = 0$ in the XXZ language) and for the Ising model (see Sec. 2.2). Dimers on the hexagonal lattice probably offer one of the simplest example. In the brick wall picture (Fig. 1.10) a dimer configuration appears as a

[30] We see here that the mutual information in a classical system is bounded by the length of the boundary, it obeys a boundary law [90].

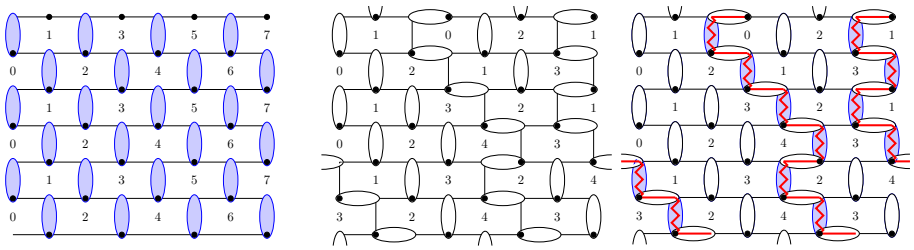

Figure 1.10: Hexagonal lattice viewed as a brick wall lattice (taken from Ref. [2]). Left : reference configuration. Middle : real configuration. Right : Transition graph with Fermion world lines. The dimers of the reference configuration are in blue. The fermions are living on the vertical edges of the lattice and are symbolized by red zigzag lines. The integers attached to each plaquette of the lattice form a height configuration associated with the dimer covering. When coarse-grained, these microscopic heights become the free field which describe the long-distance properties of the system [109]. The heights can be constructed by fixing $h = 0$ at some origin and then moving from plaquette to plaquette by turning clockwise around the sites of the even sublattice (marked with black dots). The height increases by +2 when crossing a dimer, and -1 otherwise. Since there is exactly one dimer touching each site, the height difference between two points does not depends on the chosen path (on a simply connected domain).

set of non-intersecting "world lines". These lines can be interpreted as a fermions moving up (imaginary time direction) by hopping to the left or to the right, and the total particle number is conserved. The later corresponds to the winding number in the height language. The non-intersecting condition is naturally taken into account by a fermionic statistics, and the hopping gives [2]:

$$\mathcal{T} c_j^\dagger \mathcal{T}^{-1} \quad = \quad c_j^\dagger + c_{j+1}^\dagger. \tag{1.45}$$

where $c_j^\dagger$ creates a fermion (line in the transition graph) on the vertical bond j.[31] The reference dimer configuration is the fermion vacuum (Fig. 1.10) and is invariant under the action of the transfer matrix: $\mathcal{T}|0\rangle = |0\rangle$. Going to Fourier space with $c_k^\dagger = \frac{1}{\sqrt{L}} \sum_{j=0}^{L-1} e^{-ikj} c_j^\dagger$, the Eq. 1.45 becomes

$$\mathcal{T} c_k^\dagger \mathcal{T}^{-1} = \lambda(k) c_k^\dagger \quad \text{with} \quad \lambda(k) = 1 + e^{ik}. \tag{1.46}$$

Since $\mathcal{T}$ acts independently on each Fourier mode, it can then be written explicitly as [2]:[32]

$$\mathcal{T} = \prod_k \left(1 + e^{ik} c_k^\dagger c_k\right). \tag{1.47}$$

The eigenstate of $\mathcal{T}$ with the largest eigenvalue is a Fermi sea where all the single particle states with $|\lambda(k)| > 1$ are occupied:

$$|g\rangle = \left(\prod_{k\in\Omega} c_k^\dagger\right)|0\rangle. \tag{1.48}$$

[31] The numbering on the horizontal axis is such that going from site j to site j on the upper line is a jump to the left and going from j to $j+1$ is a jump to the right.

[32] A similar derivation can be done for dimers on the square lattice, with the slight difference that a two-site unit cell is required [110, 2].

The set Ω of occupied momenta is $\Omega \simeq [-2\pi/3, 2\pi/3]$ in the thermodynamic limit, and we note $\Omega = \{k_1, \cdots, k_N\}$ on a finite lattice (for detailed finite-size formula, see [2]). $|g\rangle$ is a Fermi sea at density $\rho = N/L = 2/3$ and the associated wave function is a Slater determinant made out of N plane waves. But since the total number of particles is conserved, one can also consider other RK states corresponding to other density/winding sectors (see Sec. 1.4.4).

We wish to compute the probability of a real space configuration $|i\rangle$ of the fermions, located at positions $r_1, \cdots, r_N$. This nothing but the square of the Slater determinant [2]:

$$p_{i=\{r_1,\cdots,r_N\}} = \left|\langle 0|c_{r_N}\dots c_{r_1} c^\dagger_{k_1}\dots c^\dagger_{k_N}|0\rangle\right|^2 = \left(\frac{1}{L}\right)^N \left|\det\left(e^{-ir_j k_{j'}}\right)_{jj'}\right|^2. \quad (1.49)$$

Since the occupied momenta k_j are equally spaced, the equation above above is a Vandermonde determinant, and it simplifies to:

$$p_{i=\{r_1,\cdots,r_N\}} = \frac{1}{L^N} \prod_{1\le j<j'\le N} 4\sin^2\left(\frac{\pi}{L}(r_j - r_{j'})\right). \quad (1.50)$$

Going back to the initial RK wave function, the Eq. 1.50 gives each eigenvalue p_i of the RDM of a half-infinite cylinder. However, to get the von Neumann or Rényi entropy, we still have to sum over all the configurations i, and performing this exponential sum is in general a difficult task.[33] So, even though each probability p_i can be obtained in a polynomial time for these free fermion problems, computing exactly the associated entropy remains exponentially long in L.

1.4.4 Numerical results and subleading entropy constant

Critical dimers

We computed numerically the EE $S_1 = -\sum_i p_i \log(p_i)$ for various equal-amplitude RK states based on hard core dimer coverings. Fig. 1.11 shows the results on the hexagonal lattice for several fermion densities, as well as on the square lattice (at half filling / zero winding sector). The EE appears to grow linearly with the cylinder circumference L, which is a manifestation of the boundary law. But what is more interesting is the fact that the four states we considered obey a scaling of the form

$$S_1 \simeq \alpha L + s_1 + o(1) \quad \text{with } s_1 \simeq -0.500(1) \quad (1.51)$$

with a "slope" α which depends on the lattice and on the particle density, but the *same* subleading constant $s_1 \simeq -\frac{1}{2}$ (up to the finite-size uncertainty, see inset of Fig. 1.11). This constant is formally analog to the TEE discussed in Sec. 1.3 but the present state is critical and has algebraic dimer-dimer correlations. In addition, the subleading constant comes from a direct fit of the finite-size data, without any subtraction procedure (LW or KP) to eliminate the boundary part.

This later point deserves some further discussion. In general, the length of the boundary of a given subsystem is not completely well defined on a lattice, since different prescriptions to treat the angles would lead to (slightly) different values. This was illustrated in the case of simple circular areas on the triangular lattice in Sec. 1.3 (and Ref. [1]). An equivalent point

[33] For specific combinations of the fermion density and Rényi index, a mapping to the Dyson-Gaudin's gas allows to obtain the entropy exactly [111, 112].

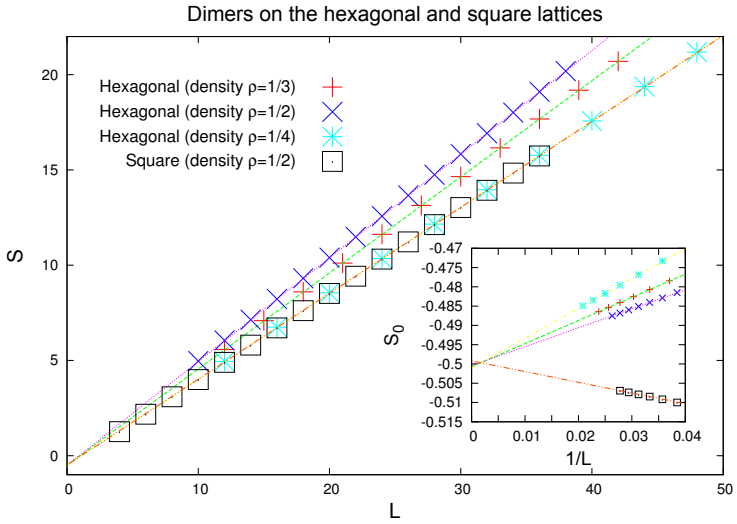

Figure 1.11: Entanglement entropy of RK states corresponding to dimer models on the hexagonal lattice (with fermion density $\rho = 1/4,\ 1/3,\ 1/2$) and the square lattice (with $\rho = 1/2$). In all cases the entropy scales as $S \simeq \alpha L + S_0 + b/L$ with $S_0 = -0.500(2)$. The inset shows the subleading constant (s_1 in Eq. 1.51) computed from system sizes in the interval $[12, L]$ as a function of $1/L$ to show the convergence towards $-0.500(1)$. Taken from [2].

of view is that each corner of the boundary contributes locally to the boundary EE. Generally speaking, the boundary EE depends on local geometric properties of the boundary, like the curvature or sharp angles. The contribution of local correlations to the EE is therefore not strictly proportional to the length of the boundary, but contains some additional contributions coming from each corner. These $\mathcal{O}(1)$ contributions get mixed with a possible *universal* subleading constant originating from *long distance* correlations. The boundary is however straight and translation invariant in a cylinder geometry. For this reason we expect the boundary EE to scale with L, without $\mathcal{O}(1)$ corrections. So, subleading entropy constants are expected not to be affected by boundary contributions in a cylinder (or torus) geometry, they are instead only sensitive the long distance properties of the system. This robustness can already be seen from the fact that different states give the same s_1 (Fig. 1.11). This will be checked on many other examples in the following sections.

Anticipating on the results of the next chapter (Sec. 2.1.2), the subleading term in the Rényi entropy turns out to be directly related to the boson compactification radius R. The present dimer wave function corresponds to $R = 1$ (free fermions) but for other values of R the subleading terms are given by :

$$S_n = \begin{cases} \alpha_n L + \log(R) - \frac{\log n}{2(n-1)} & n \leq n_c \\ \alpha_n L + \frac{n}{n-1}\log(R) - \frac{\log d}{n-1} & n > n_c \end{cases} \tag{1.52}$$

$$n_c = \frac{d^2}{R^2}, \tag{1.53}$$

where α_n is non-universal, d is the degeneracy of the configuration with highest probability and n_c a critical value of the Rényi index which separates a "phase" where the effective boundary is critical and a phase where it is massive and long-range ordered. The data of

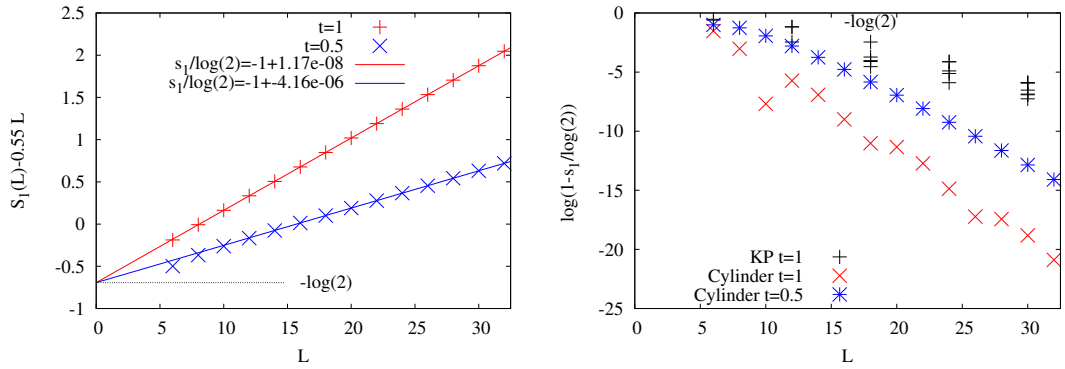

Figure 1.12: EE for dimer RK states on the anisotropic triangular lattice (data from [6]). Left: EE of a half-infinite cylincer of circumference L, for two different fugacities $t = 1$ (isotropic triangular lattice) and $t = 0.5$ (see Sec. 1.3.3). The straight lines are least-square fits to the data point with $L \geq 25$. Right: Logarithm of the difference between the estimated TEE and the exact value for dimer RK states on an anisotropic triangular lattice as a function of L. The estimate for s_1 is obtained by a fit to $aL + s_1$ for two even consecutive values of L. The convergence to $-\log(2)$ is exponentially fast, with an effective correlation length close to the dimer-dimer correlation length. For comparison we also show the data in the KP geometry, which are significantly less precise.

Fig. 1.11 correspond to $R = 1$, $d = 1$ and $n = n_c = 1$ for the square lattice, and $n = 1$, $R = 1$, $d = 1/\rho$ and $n_c = \rho^{-2}$ in the honeycomb case. In all the cases displayed in Fig. 1.11 we have $n = 1 \leq n_c$ and therefore, using Eq. 1.52, we find $s_1 = -\frac{1}{2}$, in agreement with the numerics.

It is possible to vary the compactification radius R of these RK dimer wave functions by adding some dimer-dimer interaction in the classical Boltzmann weights, as was done on the square lattice [113]. In such interacting case the transfer matrix is no longer a free fermion problem but can still be diagonalized numerically (Lanczös) to get the p_i for some finite L. This would allow to check the Eq. 1.52 for $R \neq 1$. This has not been carried out but we present some other checks for various R and n in the next chapter.

Gapped $\mathbb{Z}_2$ dimer liquid and exponential convergence to $\gamma = \log(2)$

The previous paragraph explained (heuristically) why the cylinder geometry allows for a direct measurement of the "universal"[34] subleading entropy constant. But this idea is not restricted to critical states and can also be used to measure the TEE introduced in Sec. 1.3. For instance, it is possible possible to compute the p_i for dimers on the triangular lattice and therefore to obtain the EE of a half-infinite system in the gapped $\mathbb{Z}_2$ phase. We observe an almost perfect $S_1 \simeq \alpha L + s_1$ scaling and the subleading s_1 is very close to $-\log(2)$.[35] The accuracy on s_1 is shown in Fig. 1.12 as a function of the number of boundary sites (proportional to the circumference L of the cylinder). We observe that the convergence is exponentially fast, in

[34] Here the meaning of universal is simply "insensitive to the effects of local correlations".

[35] The observation that a translation invariant boundary allows for a direct determination of universal subleading constants was made in Ref. [1], where the TEE could be obtained with a much higher precision on a torus than using the KP/LW schemes. The cylinder geometry is now widely used by the community for computing numerically the TEE, also because it is adapted to the DMRG simulations (see for instance [32]). See also [42] for an application in the continuum (FQHE).

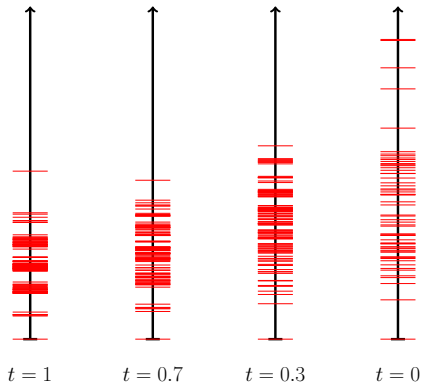

Figure 1.13: Entanglement spectrum for dimer RK states on the (anisotropic) triangular lattice with circumference $L = 12$, for various fugacities. Left: isotropic triangular lattice. Right: square lattice (critical point). From [6].

$\sim \exp(-L/\xi)$, which is what we expect from the argument of the previous paragraph in the case of a translation-invariant boundary and finite correlation length.

1.4.5 Entanglement spectrum

The spectrum of a RDM contains more information than the just the EE, as was pointed out for fractional quantum Hall states [35]. It is thus natural to look in more detail at the classical probabilities $\{p_i\}$. However, the (constrained) RK states have the particular property that each eigenstate of the (half cylinder) RDM is a single classical configuration (and not a linear combination of several configurations). Due to the translation invariance along the boundary, these configurations can be translated to give a set of exactly degenerate eigenvalues. So, the ES contains some flat bands. This is somehow an annoying feature of these states because we cannot use lattice momentum to visualize the spectrum or to identify dispersing modes. It is nevertheless instructing to look at the associated density of states, and Fig. 1.13 provides three examples of ES, where an "energy" $E_i = -\log(p_i/p_{\max})$ was associated to each probability. An interesting observation is that the entanglement gap grows when going from the liquid state on the isotropic triangular lattice to the critical point (square lattice), contrary to the energy gap which, of course, vanishes at $t = 0$ in the thermodynamic limit. It is in fact easy to show that the entanglement gap is finite at the critical point ($t = 0$) in the thermodynamic limit, since it can be computed exactly: $-\log(p_1/p_{\max}) = 2\log(\pi)$ [6]. A finite entanglement gap is expected to be the generic situation for RK states, precisely because it is the ratio of the classical probabilities of two boundary configurations which have to differ (at least) locally (see also the argument of Ref. [114]).

According to the bulk-edge correspondence ideas [35], the ES of a system system which is gapped in the bulk reflects the energy of physical edge modes (if any) which would appear if the system had a physical boundary. The present dimer RK states are indeed gapped in the bulk for $t \neq 0$, but they are not chiral and presumably do not show any gapless edge modes (unlike topological insulators or quantum Hall states). This is how one can reconcile the bulk-edge correspondence and the presence of a gap in the ES.

Chapter 2

Shannon-Rényi entropy of spin chains

The motivation of the previous chapter was to understand the RDMs and EE in 2D RK states. One outcome was that, in a long (half) cylinder geometry, the spectrum $\{p_i\}$ of the RDM is contained in one state $|g\rangle$, which is the dominant eigenvector of the classical transfer matrix $\mathcal{T}$ (Sec. 1.4). Furthermore, it was found that for some dimer RK states on the hexagonal lattice, $|g\rangle$ is a Fermi sea. This suggests to consider the boundary of the half cylinder as a quantum chain, and to interpret the EE of the RK state as the Shannon entropy of its wave function.[1] In other words, a many-body state $|\psi\rangle$ is expanded in some local basis $\{|i\rangle\}$: $|\psi\rangle = \sum_i \psi_i |i\rangle$. And we then define its Shannon-Rényi entropy (SRE), *in that basis*, to be

$$S_n = \frac{1}{1-n} \log \left(\sum_i p_i^n \right) \quad \text{with} \quad p_i = |\psi_i|^2 = |\langle \psi | \, i \rangle|^2 \,, \tag{2.1}$$

without any reference to some 2D system. At this point, at least three natural questions arise: is it useful and/or interesting to study the Shannon entropy of a quantum system in 1+1 dimension ? What about the basis dependence ? Is there some relation to the (basis independent) EE of some subsystem in the chain ?

For one-particle problems described by a wave function $\psi(r)$ in real space, the entropy above is equivalent to so-called inverse participation ratios : $P_n = \int d^D\mathbf{r} \, |\psi(r)|^{2n}$. The later measure how spatially localized is the particle. In presence of disorder it can be used detect Anderson metal-insulator transitions [115]. In the delocalized phase one has $P_n \simeq L^{-D(n-1)}$, where D is the spatial dimension. In the localized phase one has instead $P_n \simeq L^0$. At the transition point it scales like $P_n \simeq L^{-\alpha_n(n-1)}$ where α_n defines a continuous family of critical exponents (multifractality). In the notation of Eq. 2.1 it means $S_n \simeq \alpha_n \log(L)$.

On the other hand, a generic – not necessarily critical – many-body wave function has some non-zero weights on a large fraction of the basis states, and we thus expect the leading behavior of the SRE (Eq. 2.1) to be a *volume law*, which means $S_n \simeq \alpha_n L$ for a chain of length L.[2] Although this could also be interpreted as "multifractality" [116][3] the informations about the long-distance properties of the system are available in the subleading terms, as for the EE

[1] *Shannon* entropy simply means here that we associate $-\sum_i p_i \log p_i$ to some set of probabilities $\{p_i\}$.

[2] In the 2D RK point of view, this $\mathcal{O}(L)$ scaling was a boundary law for the EE.

[3] Contrary to one-body wave function in real-space, multifractality is generic for wave functions living in a many-body Hilbert space, even for featureless product states. Consider for instance N inde-

discussed in the previous chapter. We found that these subleading corrections are typically $\mathcal{O}(1)$ for periodic chains [2], and $\mathcal{O}(\log L)$ for open chains [117, 5]. In Ch. 3 we will also discuss the occurrence of $\mathcal{O}(\log L)$ for periodic systems in 2D.

Since here we no longer require any connection to the EE of some higher dimensional RK state, one can also consider the SRE S_n^Ω of a *subsystem* Ω. It is formally very similar to the SRE of the full system: $S_n^\Omega = \frac{1}{1-n}\log\left(\sum_j p_j^n\right)$ but the subsystem probabilities p_j are the diagonal elements of the RDM: $p_j = \langle j|\,\rho^\Omega\,|j\rangle$. These partial SRE have a dominant behavior which is proportional to the volume of the subsystem and, contrary to the EE, the partial SRE is not the same for one subsystem Ω and its complement $\bar\Omega$. It is convenient to study the combination $I_n(\Omega,\bar\Omega) = S_n^\Omega + S_n^{\bar\Omega} - S_n^{\Omega\cup\bar\Omega}$, called Shannon-Rényi mutual information, since the extensive contributions cancel out, and one is left with universal subleading terms. In particular, for a segment in a longer critical chain, the mutual information I_n is $\mathcal{O}(\log L)$ [111, 118, 112].

We conclude this brief overview on SRE by mentioning a related point of view, which is to introduce a deformation $|\psi,n\rangle$ of the wave function $|\psi\rangle$, that may be called "Rényification". It is defined by:[4]

$$|\psi,n\rangle = \frac{1}{\sqrt{Z(n)}}\sum_i (p_i)^{n/2}\,|i\rangle \tag{2.2}$$

$$\text{with } Z(n) = \sum_i (p_i)^n\,. \tag{2.3}$$

This Rényified state can then be used to compute correlation functions. This definition immediately brings numerous questions: are the long-distance properties of $|\psi,n\rangle$ different from those of $|\psi\rangle = |\psi,1\rangle$? If $|\psi,n\rangle$ has some algebraic correlations, do the associated exponent(s) change with n ? Is there a phase transition as a function of n ? What parent Hamiltonian would have $|\psi,n\rangle$ as a ground state ? Do we learn something about $|\psi\rangle$ by studying $|\psi,n\neq 1\rangle$. What are the interesting basis choices ? Although we have no general answer to these questions, this chapter will shed some light on these issues through a few specific examples and results.

2.1 XXZ spin chain and compactified free boson

We now discuss the (full system) SRE of a specific model, the XXZ spin chain. It is defined by the following Hamiltonian:

$$H = -\frac{1}{2}\sum_i \left(S_i^+ S_{i+1}^- + \text{H.c}\right) + \Delta\sum_i S_i^z S_{i+1}^z. \tag{2.4}$$

Its ground state is critical for $|\Delta|\leq 1$ and is the prototype of Tomonaga-Luttinger (TL) liquid. Correlation functions decay algebraically at zero temperature [119]:

$$\begin{aligned}\langle S_0^z S_x^z\rangle &\simeq ax^{-2} + b(-1)^x x^{-2K} + \cdots\\ \left\langle S_0^+ S_x^-\right\rangle &\simeq cx^{-\frac{1}{2K}} + d(-1)^x x^{-2K-\frac{1}{2K}} + \cdots\end{aligned} \tag{2.5}$$

pendent spin-$\frac{1}{2}$ in the same state $\cos(\theta)|\uparrow\rangle + \sin(\theta)|\downarrow\rangle$. The SRE of that tensor product state is $S_n = \frac{N}{1-n}\log\left(\cos(\theta)^{2n} + \sin(\theta)^{2n}\right)$, which is a non-linear function of n.

[4] $|\psi\rangle$ is assumed to be real and positive in the $|i\rangle$ basis. If not, the following definition of the Rényified state would allow to preserve the sign or complex phases of the original state: $|\psi,n\rangle = \sum_i (p_i)^{(n-1)/2}\,\langle i|\,\psi\,\rangle\,|i\rangle$.

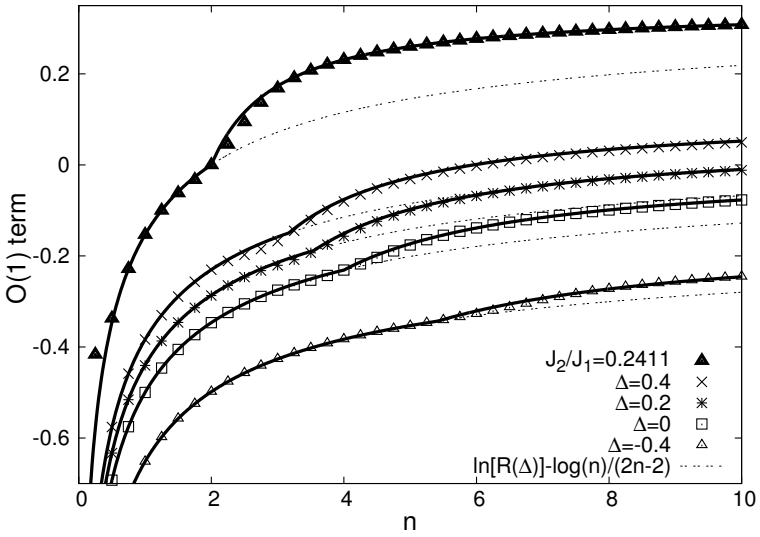

Figure 2.1: Constant term in the SRE of periodic XXZ and $J_1 - J_2$ chains for different values of Δ and at the critical point $J_2/J_1 = 0.2411$. Each point comes from fitting the data for $L = 20, 22, 24, 26$ and 28 to $aL + b + c/L + d/L^2$. Fat lines: theoretical prediction (Eq. 1.52). The prediction for $n < n_c$ is also plotted above n_c (dashed lines) for comparison. The $J_1 - J_2$ chain ($SU(2)$ symmetric, but with second neighbor interaction) lies at the transition point between a TL liquid phase and a dimerized one. It has $R = \sqrt{2}$, as the XXZ chain at $\Delta = 1$, but no logarithmic corrections (hence smaller finite-size effects). Taken from [5].

where a, b, c, d are (non-universal) constants and K is the Luttinger parameter. The fact that the Hamiltonian is integrable makes it possible to relate K to the microscopic anisotropy parameter:

$$\frac{1}{K} = R^2 = 2\left(1 - \frac{\arccos(\Delta)}{\pi}\right) \tag{2.6}$$

where R is the effective compactification radius.

2.1.1 Numerics on periodic chains

First of all we need to choose some local basis to expand the wave function. Since $S^z_{\text{tot}} = \sum_{i=0}^{L-1} S^z_i$ is a conserved quantity, a natural choice is the "Ising basis", where basis states are eigenstates of the S^z_i. In the particle language, these basis states are configurations where each particle has a fixed position, which also sounds natural from a classical statistical mechanics point of view.

We computed numerically the ground state of the XXZ Hamiltonian using Lanczös diagonalization in the S^z_i basis on small periodic chains ($L \leq 28$). The probabilities p_i are obtained directly as the square of the ground state components, and an explicit summation over the non-zero weights gives $S_n(L)$, possibly for non-integer n.

As discussed in the previous chapter, a fit is enough to extract universal subleading terms when the system is translation invariant, and the subleading corrections are here $\mathcal{O}(1)$. Some

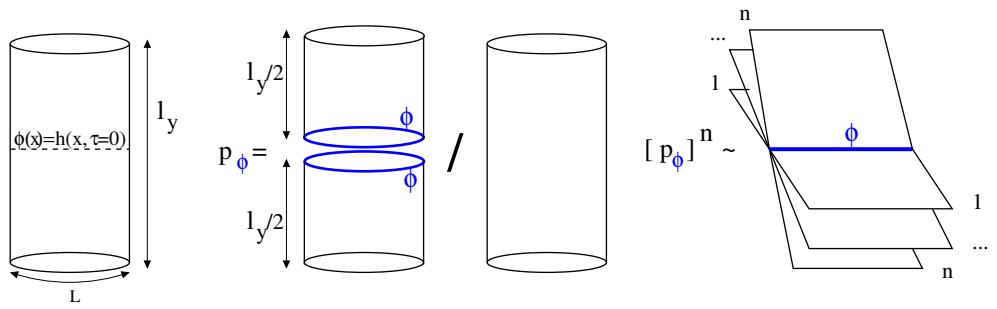

Figure 2.2: Left: $\phi(x)$ is the value of the height field $h(x,\tau)$ at $\tau = 0$. Center: The probability p_ϕ of a given ϕ is the ratio of partition function with and without constrain on $h(x, \tau = 0)$. Right: If $2n$ is an integer, $(p_\phi)^n$ involves the partition function on a "book" geometry, where the $2n$ sheets are independent except at $\tau = 0$ where h must match $\phi(x)$ (binding).

results are displayed in Fig. 2.1 for various values of Δ and n. We observe a very good agreement with the theoretical prediction announced in Eq. 1.52, including a "cusp" at some critical value n_c of the Rényi index (given by Eq. 1.53). We now turn to the theoretical derivation of Eq. 1.52 using a (free) field theory argument.

2.1.2 Gaussian trick and CFT book

We present here a derivation of Eq. 1.52, using a slightly expanded version of the argument given in [5]. The idea is to exploit the Gaussian nature of the action in the continuum limit to perform the summation over probabilities which appears in the definition of the SRE. This approach does not require $2n$ to be an integer and also allows to understand the presence of a critical value of the Rényi index, which a more standard replica approach would not capture.

This method transforms the calculation of the subleading term of the SRE into a ratio of simple cylinder partition functions with Dirichlet boundary condition, which is a standard boundary CFT quantity [93, 120]. Boundary field theory has found many applications in the study of quantum impurity problems in 1D [93], and there the boundary corresponds to a spatially localized impurity. In space-time, the boundary is thus parallel to the imaginary-time axis. It is interesting to note that here, instead, the boundary will be parallel to the real-space axis (see [121] for another example).

$n \leq n_c$

The long distance and low energy properties of a TL liquid are described by a compactified "height" field $h(x,\tau)$ which Euclidean action is Gaussian and reads :

$$S[h] = \frac{\kappa}{4\pi} \int dx d\tau (\nabla h)^2 \tag{2.7}$$

$$\mathcal{Z} = \int \mathcal{D}[h] \ \exp\left(-S[h]\right). \tag{2.8}$$

where κ is the stiffness and r is the compactification radius ($h \equiv h + 2\pi r$). By rescaling the height field one can change r and κ, but the the physical observables only depend on the combination $2\kappa r^2$, which stays constant upon rescaling. The parameter which fixes the decay exponents of the correlations functions is $R^2 = 2\kappa r^2 = 1/K$. Since r will not be used

explicitly in what follows, we will call R the compactification radius. For a periodic chain at zero temperature, h lives on an infinitely long cylinder of perimeter L.

The entropy we are interested in is based on probabilities p_i computed in a particular basis, here the S^z basis. But the continuum limit of an S^z operator is local and diagonal in the height basis [119]. So, the height basis is the continuum limit of the Ising basis,[5] and the microscopic probabilities p_i may be replaced by the probabilities p_ϕ of field configurations $\phi(x) = h(x, \tau = 0)$.

One can obtain the probability (density) p_ϕ by integrating the fluctuations of h with a fixed boundary condition at $\tau = 0$ (see Fig. 2.2).[6] But, even without doing the calculation explicitly, we know that the result should be a Gaussian functional for ϕ, with a one-dimensional inverse propagator proportional to κ.[7] We can therefore write:

$$p_\kappa[\phi] = p_{\kappa,\max} \exp\left(-\frac{\kappa}{2} \sum_{0\le x,x'<L} \phi_x G^{-1}_{x,x'} \phi_{x'}\right) \tag{2.9}$$

where we explicitly kept track of the stiffness κ and the normalization factor was expressed in term of the probability $p_{\kappa,\max} = p_\kappa[\phi = 0]$ of the "Dirichlet configuration" $\phi(x) = 0\ \forall x$. We can now raise $p_\kappa[\phi]$ to some arbitrary power n:

$$(p_\kappa[\phi])^n = (p_{\kappa,\max})^n \exp\left(-\frac{n\kappa}{2} \sum_{0\le x,x'<L} \phi_x G^{-1}_{x,x'} \phi_{x'}\right). \tag{2.10}$$

Using again Eq. 2.9, but for a different value $\kappa' = n\kappa$ of the stiffness, we can express the Gaussian factor of Eq. 2.10:

$$\exp\left(-\frac{n\kappa}{2} \sum_{0\le x,x'<L} \phi_x G^{-1}_{x,x'} \phi_{x'}\right) = \frac{p_{n\kappa}[\phi]}{p_{n\kappa,\max}}. \tag{2.11}$$

Combining Eq. 2.10 and 2.11 we get:

$$(p_\kappa[\phi])^n = (p_{\kappa,\max})^n \frac{p_{n\kappa}[\phi]}{p_{n\kappa,\max}}. \tag{2.12}$$

But the probabilities are normalized, $\sum_\phi p_{n\kappa}[\phi] = 1$. Summing over all the field configurations is therefore straightforward:

$$Z(n) = \sum_\phi (p_\kappa[\phi])^n = \frac{(p_{\kappa,\max})^n}{p_{n\kappa,\max}}. \tag{2.13}$$

At this point we have reduced the calculation of the entropy $S_n = \frac{1}{1-n} \log Z(n)$ to the evaluation of $p_{\kappa,\max}$ for two different values of the stiffness, κ and $\kappa' = n\kappa$. Or equivalently, two

[5] This correspondence is the same to that between the microscopic dimer configurations on the hexagonal (or any bipartite) lattice (and therefore XX spin chain at the boundary) and the coarse-grained height field (for a definition of the microscopic heights, see Fig. 1.10 and caption).

[6] To make each probability finite some regularization is necessary but the present argument does not require to consider it explicitly.

[7] In the present case G^{-1} is $\sim k$ in momentum space, $G(x) \sim \log|x|$ and $G^{-1}(x) \sim x^{-2}$ in real space.

values of the radius: the original radius R, and an effective radius $R' = \sqrt{n}R$. As illustrated in Fig. 2.2, this probability is given by $p_{\max} = \lim_{l_y \to \infty} [Z_{DD}(l_y/2)]^2 \, Z_{DD}(l_y)^{-1}$, where $Z_{DD}(l)$ denotes the partition function of a cylinder of height l with Dirichlet boundary conditions at both ends.[8] If these partition functions were regularized using some lattice model for instance, $\log p_{\max}$ would contain some non-universal extensive part $\mathcal{O}(L)$. But we are instead interested in universal subleading terms, and these terms are precisely those described by CFT. In fact the ratio of partition functions appearing above is a well studied object in CFT and the $l_y \to \infty$ limit it is equivalent to an Affleck-Ludwig g-factor (or "ground state degeneracy") [93]. In the present compactified free-field case the relevant g-factor is g_D, associated with a Dirichlet boundary:

$$p_{\max} = \lim_{l_y \to \infty} \frac{[Z_{DD}(l_y/2)]^2}{Z_{DD}(l_y)} \quad = \quad (g_D)^2 \, . \tag{2.14}$$

g_D has been computed [120] and is a simple function of R:

$$g_D = R^{-1/2} = \left(2\kappa r^2\right)^{-1/4} \tag{2.15}$$

Combining Eqs. 2.13-2.14 with Eq. 2.15 gives $Z(n) = \frac{R'}{R^n}$ with $R' = \sqrt{n}R$, and finally:

$$Z(n) \quad = \quad \sqrt{n} R^{1-n} \tag{2.16}$$

$$S_n = \frac{1}{1-n} \log\left[Z(n)\right] \quad = \quad \log(R) - \frac{\log(n)}{2(n-1)}. \tag{2.17}$$

which is equivalent to Eq. 1.52 when $n \leq n_c$. We have checked this results numerically using the XXZ chain, at zero and non-zero magnetizations, as well as in $J_1 - J_2$ chain [2]. Luitz *et al.* [54] have also checked this result for an Heisenberg two-leg ladder at finite magnetization, another example of TL liquid.

The above arguments do not require $2n$ to be integer – it is a "replica-free" argument. However, if $2n$ is an integer, $Z(n)$ can be interpreted as the partition function of a "book" (right of Fig. 2.2) with $2n$ sheets that are glued together at $\tau = 0$. This provides a simple representation for the Rényified state defined in Eq. 2.2: correlation functions measured in the state $|\psi, n\rangle$ are nothing but the classical correlations measured along the binding of the book.

This approach can also be compared to that of Fradkin and Moore [20]. They treated the book partition function by forming some linear combinations of the n scalar fields living on the n (double) sheets. They introduced $n-1$ "difference" fields: $\delta h_i = \frac{1}{\sqrt{2}}(h_i - h_{i+1})$ and one "center of mass" field: $H = \sum_{i=1}^{n} h_i$. They treated these new fields as independent from each other, which implicitly means that some compactification conditions are neglected (see Oshikawa [122] for a proper construction of the boundary state in the compactified case). In this approximation, the book partition function becomes that of $n-1$ independent difference fields obeying a Dirichlet boundary condition at $\tau = 0$, and one unconstrained field (H). In our notations their results is $Z(n) = p_{\max,\kappa}^{n-1}$. Comparing to Eq. 2.13, the treatment of Ref. [20] appears to be incorrect concerning the contributions which depend on the compactification radius (or κ). However, in geometries with corners (see Sec. 2.1.3), the leading universal term in the SRE is a logarithm which coefficient is independent of R, and is therefore given correctly by the approach of [20].

[8] We assumed here for simplicity that the boundary conditions at $\tau = \pm\infty$ are also of Dirichlet type.

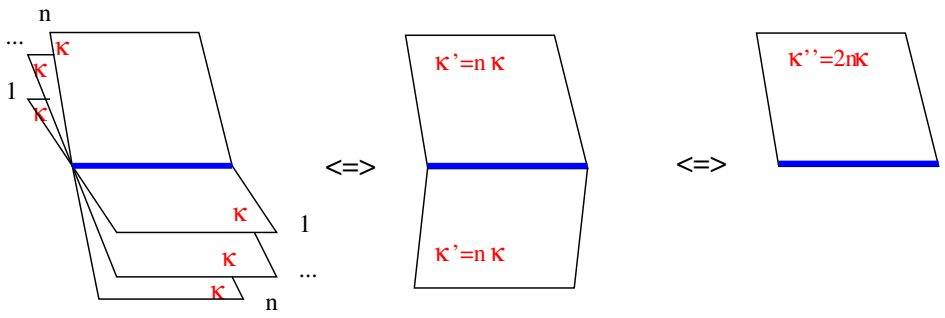

Figure 2.3: Below n_c the book partition function $Z(n)$ is equivalent to that of a of a double-sheet book with modified stiffness $\kappa' = n\kappa$, or to that of a single-sheet with modified stiffness $\kappa'' = 2n\kappa$. A perturbation (cosine potential) along the book binding is therefore equivalent to a conventional boundary perturbation provided we use an effective stiffness $\kappa'' = 2n\kappa$.

$n = n_c$

The argument above works as long as the effective action describing the subleading terms in the SRE is Gaussian. However, at the microscopic scale the system lives on a lattice and the action is not strictly Gaussian but contains all the possible terms allowed by symmetry. Among these terms, the cosine potentials $\cos(d \cdot h(x,\tau)/R)$ play an important role (vertex operators). They are compatible with the compactification condition $h \equiv h + 2\pi r$ and have d minima. The (bulk) scaling dimension of such an operator is $x_{\text{bulk}} = \frac{d^2}{R^2}$ (recall that $R = \sqrt{2\kappa r}$) and it is irrelevant (RG sense) when $x_{\text{bulk}} > 2$.[9] We only need to consider the most relevant of these operators and d is therefore the smallest degeneracy allowed by symmetry. For the XXZ chain at zero magnetization $d = 2$.[10]

Let us analyze the effect of the cosine potential in the partition function $Z(n)$. We assume that $2n \in \mathbb{N}$ so that $Z(n)$ can be viewed as book partition function (Fig. 2.3), although the final result is in fact valid without this restriction. Since the spin chain is critical, the cosine potential is irrelevant (or marginal) when it perturbs the *bulk* of the 2D action. So the cosine potential renormalizes to zero at long distances in the bulk of the sheets of the book. For $n = 1$ the book is nothing but the usual plane, so the cosine term can be certainly be ignored in the 2-sheet book. But this may not be the case along the *binding* of the book for $n \neq 1$. The scaling dimension of an operator is different when it acts along a one-dimensional boundary [123]. For a vertex operator, the boundary scaling dimension is $x_{\text{boundary}} = 2\, x_{\text{bulk}} = \frac{2d^2}{R^2}$, and when

$$x_{\text{boundary}} = 1 \tag{2.18}$$

the operator is marginal at the boundary of a half-plane plane.[11] What about the effect of such a perturbation at the binding of a book with $2n$ sheets ? Using the Gaussian trick, the

[9] This result can be recovered by a simple perturbative RG calculation.

[10] In the XXZ spin chain at zero magnetization, the most relevant (smallest d) cosine term has $d = 2$ and this operator becomes relevant for $x = 4/R^2 < 2$, that is $R > \sqrt{2}$. The transition point corresponds to the $SU(2)$ symmetric point (Heisenberg) at $\Delta = 1$. For $R > \sqrt{2}$ the height field is effectively "locked" in one of the two degenerate minima, which are the continuum counterparts of the two antiferromagnetic Ising configurations $\uparrow\downarrow\uparrow\cdots$ and $\downarrow\uparrow\downarrow\cdots$.

[11] The factor two between x_{boundary} and x_{bulk} can be obtained as an immediate consequence of the equivalence between the center and right panels of Fig. 2.3. The correlations of the cosine term at the boundary (right panel) of a system with stiffness κ'' are the same as those of the cosine operator in the bulk of a system with stiffness $\kappa' = \kappa''/2$ (center panel). Hence: $x_{\text{boundary}}(\kappa'') = x_{\text{bulk}}(\kappa''/2) = 2x_{\text{bulk}}(\kappa'')$.

statistics of $\phi(x)$ at the binding of the book is mapped to that at the boundary of a single sheet (right of Fig. 2.3), with a modified n-dependent stiffness $\kappa'' = 2n\kappa$. We can therefore apply the criterion of Eq. 2.18 to the geometry displayed in right of Fig. 2.3, which corresponds to an effective compactification radius $R' = \sqrt{2n}R$. The condition for the perturbation to be marginal at the binding of the book with $2n$ sheets is thus $x_{\text{boundary}}(\kappa'' = 2n\kappa) = \frac{2d^2}{2nR^2} = 1$. We finally get the critical value of the Rényi index:

$$n_c = \frac{d^2}{R^2}. \tag{2.19}$$

So, when increasing n from 1 to n_c the critical height fluctuations along the book binding are gradually suppressed. When reaching $n = n_c$ these fluctuations are weak enough that the cosine potential is marginal at the book binding, this signals the presence of a boundary phase transition. So, for $n < n_c$, raising the probabilities p_i to the power n is equivalent to consider the boundary of a single sheet with an effective stiffness $\kappa'' = 2n\kappa$ (Fig. 2.3), or one line in the bulk of a 2-sheet book at $\kappa' = n\kappa$. If we admit that the Gaussian argument is still valid *at* n_c, we are left with a boundary problem where a cosine potential is exactly marginal, which is an exactly solvable model [124].

We stress that the correct value of n_c is not given by a bulk criterion $x_{\text{bulk}}(\kappa' = n\kappa) = 2$ because it is only along the book binding that the height fluctuations are described by a modified effective stiffness κ' or κ''. Indeed the stiffness is independent of n in the bulk of the sheets, and no transition can occur there when varying n. In particular we checked numerically in the XXZ chain that in the interval $n_c/2 < n < n_c$ the Rényified state $|\psi, n\rangle$ has some algebraic $\langle S^z_0 S^z_x\rangle$ correlations (Eq. 2.5) which are described by a compactification radius $R' = \sqrt{n}R$ which is *larger* than the maximal value $\sqrt{2}$ one can get in $|\psi\rangle$ by varying the anisotropy Δ [125]. These is a bit counter intuitive since, in this regime, $|\psi, n\rangle$ has some algebraic correlations $\langle S^z_0 S^z_x\rangle \sim x^{-\eta}$ which decay very slowly, with an exponent $\eta < 1$. This exponent can go as low as $\eta = 1/2$ when approaching n_c.[12] There is however no contradiction between having such a slow decay and still being critical since $|\psi, n > 1\rangle$ is not the ground state of an Hamiltonian with short-range interactions.

$n > n_c$

Above n_c the cosine potential is relevant at the book binding, and one can no longer compute $Z(n)$ using a Gaussian action; and the Eq. 2.17 cannot be used for $n > n_c$. However, the effect of a relevant cosine potential is intuitively simple: apart from short-distance fluctuations, ϕ is locked into one of the d (spatially flat) minima of the potential.[13] As a result, the sheets are decoupled from each other. In each sheet the field $h(x, \tau)$ obeys a Dirichlet boundary condition at $\tau = 0$. As far as the universal $\mathcal{O}(1)$ term is concerned, $Z(n)$ is thus given by the d flat configurations which minimize the cosine potential:

$$Z(n > n_c) = d\,(p_{\kappa,\max})^n \tag{2.20}$$
$$= d\,R^{-n}. \tag{2.21}$$

[12] Presumably for this reason, the transition was incorrectly located at $n_c/2$ in Ref. [126].

[13] We focus here on periodic chains (each sheet is a half-infinite cylinder) where the precise locations of these minima on the compactification circle are immaterial. They however play an important role in open chains, as discussed in [6].

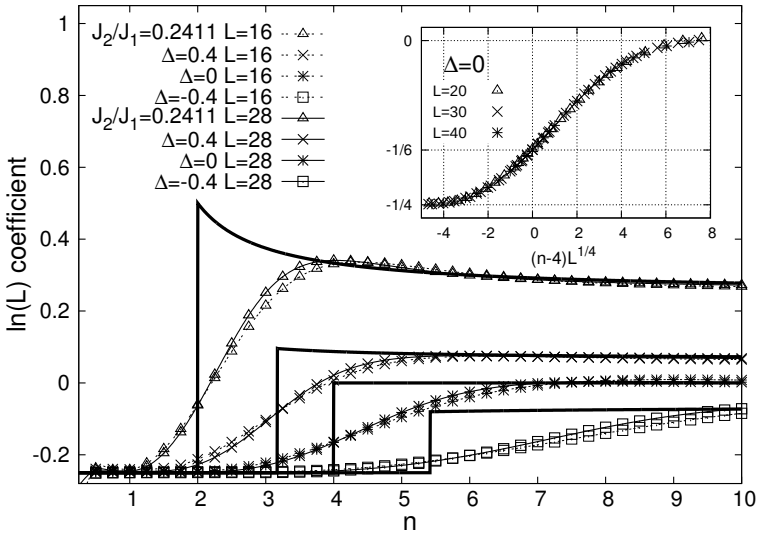

Figure 2.4: Coefficient of the $\log L$ term in the SRE of open XXZ (and $J_1 - J_2$) chains, extracted using $S_n \simeq aL + b \ln L + c + d/L$ with four even consecutive systems sizes $(L, \cdots, L-6)$ with $L = 16$ and $L = 28$. Fat lines: Eq. 2.24. Inset: scaling close to $n_c(\Delta = 0) = 4$, where we observe a coefficient very close to $-\frac{1}{6}$ and a slowly diverging slope $\sim L^{1/4}$. Taken from [5].

And finally:

$$S_{n>n_c} = \mathcal{O}(L) + \frac{\log d}{1-n} + \frac{n \log R}{n-1}, \tag{2.22}$$

which is the result announced in Eq. 1.52. Although the subleading term is continuous across the transition (Eq. 2.22 matches Eq. 2.17 if $n = n_c = d^2/R^2$), a change in the slope is clearly visible on the numerical data of Fig. 2.1.

We see that studying $|\psi, n\rangle$ for $n > 1$ can reveal the effect of some perturbation which was irrelevant at $n = 1$. What was just some short-distance fluctuations at $n = 1$ became a true long-range order above n_c. In a different context where the phase diagram of the model would not be completely known, we can imagine that looking at the Rényified states $|\psi, n\rangle$ could help identifying some competing order(s), without actually changing the Hamiltonian.

2.1.3 Logarithms in open chains and partial SRE

We have explained the origin of a universal $\mathcal{O}(1)$ term in the SRE of periodic chains. In open chains, as well as in the partial SRE of a subsystem (segment), the universal part of the SRE is a logarithm of the system/subsystem size.

Open XXZ chain

Open chains can be analyzed in a similar way to periodic ones and we only give here the main ideas. In the open cases, each sheet of the book is a semi-infinite strip. So, each sheet has

two corners with angles $\pi/2$. From the classic work of Cardy and Peschel [101] it is known that sharp corners produce logarithmic terms in the associated free energy. It is therefore not surprising that $\log(L)$ terms arise in the SRE [117, 5]. Indeed, exactly as in the periodic case, the Gaussian trick can be applied when $n < n_c$ and it reduces the book problem to a single sheet partition function with Dirichlet condition ($p_{\max}$) and n-dependent stiffness. Also, the same vertex operator becomes marginal at n_c, and for $n > n_c$ the sheets decouple from each other. This gives a discontinuity at $n = n_c$ in the coefficient l_n of the $\log(L)$ term:

$$S_n^{\text{open}} \simeq \alpha_n L + l_n \log(L) + \mathcal{O}(1) \tag{2.23}$$

$$l_n = \begin{cases} -\frac{1}{4} & n < n_c \\ ? & n = n_c \\ \frac{n}{n-1}\left(\frac{R^2}{4} - \frac{1}{4}\right) & n > n_c \end{cases} \tag{2.24}$$

Although the $\mathcal{O}(1)$ is continuous at n_c, the coefficient l_n is not. Furthermore, our numerical results suggest that, in the thermodynamic limit, $l_{n=n_c}$ is distinct from the values just above and just below the transition. For instance, we found numerically $l_{n=n_c=4} = -1/6$ in the XX chain ($\Delta = 0$, $R = 1$) (inset of Fig. 2.4), a result which has been recently confirmed by an exact calculation [112]. We are not aware of a theoretical prediction for the value of $l_{n=n_c}$ away from the free fermion point.

Entropy of a segment

Another interesting quantity is the partial SRE of a segment of length l embedded in a longer periodic chain of length L. In a recent work J.-M. Stéphan [112] showed that it obeys a conformal scaling very similar to that of the EE:

$$I_n(l, L) = \frac{1}{4} b_n \log\left(\frac{L}{\pi} \sin\frac{\pi l}{L}\right) + \mathcal{O}(1). \tag{2.25}$$

But, contrary to the EE (and contrary to the conclusions of [118]) b_n is in general *different* from the central charge. Using arguments (Gaussian action) similar to those developed in this chapter he showed in particular that, for the XXZ chain (and probably any TL liquid state), $b_{n<n_c} = 1$ and $b_{n>n_c} = \frac{n}{n-1}$, with the same critical $n_c = d^2/R^2$. The case of the Ising universality class, which is discussed in the next section, is even more intriguing, with $b_{n_c=1} = 0.4801629(2)$ [112], a number which has not yet been calculated nor identified using CFT tools.

2.2 Ising chain in transverse field

The previous section described our analytical understanding of the universal contributions to the SRE of a TL liquid, which is based on the free compactified boson description. We now turn to the next simple universality class, the 2D Ising universality class. Its simplest 1+1D realization is the Ising chain in transverse field (ICTF):

$$H = -\mu \sum_i \sigma_i^x \sigma_{i+1}^x - \sum_i \sigma_i^z, \tag{2.26}$$

where $\mu = \mu_c = 1$ corresponds to the gapless critical point separating two gapped phases: the ordered phase for $|\mu| > 1$ ($\langle \sigma^x \rangle \neq 0$) and the disordered/paramagnetic phase for $|\mu| < 1$

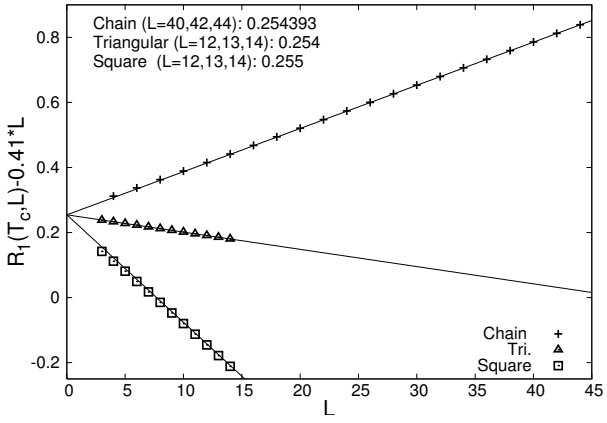

Figure 2.5: Shannon entropy of three Ising models at the critical point, plotted as a function of L (a linear term, $-0.41L$, has been subtracted for clarity). Data for the 2D square and 2D triangular lattices and for the ICTF are compared. The entropy is well fitted by $\simeq aL+r_1+b/L$ and the subleading constant r_1 is evaluated using the three largest sizes. Taken from [4].

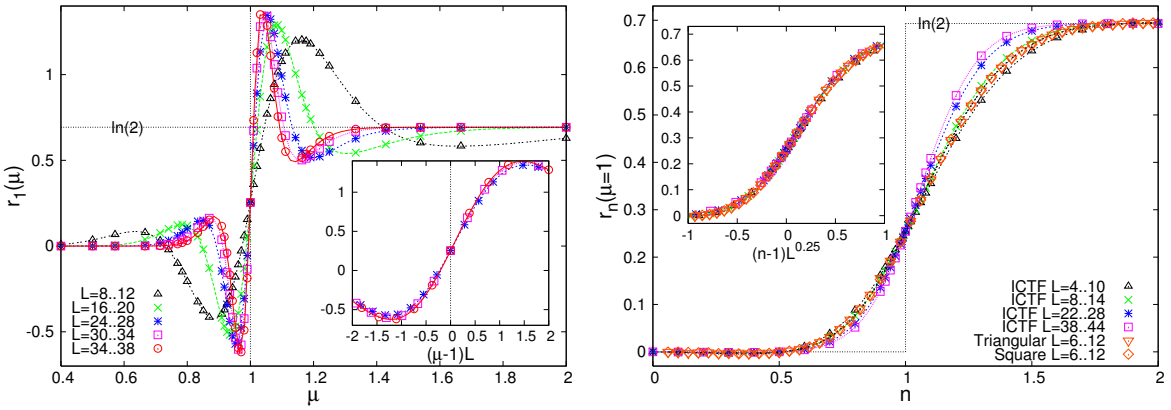

Figure 2.6: Subleading entropy constant for the Ising model (ICTF) as a function of μ with fixed $n = 1$ [$r_1(\mu)$, left panel] and as a function of n with fixed $\mu = 1$ [$r_n(\mu = 1)$, right panel]. Left inset: $r_1(\mu)$ for different system sizes, plotted as a function of $(\mu - 1)L$. The apparent collapse with $(\mu - 1)L$ on the horizontal axis suggests a infinite slope at $\mu = 1$ in the thermodynamic limit. Right inset: when plotted as a function of $(n - 1)L^{0.25}$, the data collapse reasonably well onto a single curve. If this is not a finite-size artifact... it indicates an infinite slope at $n = 1$. Taken from [4].

($\langle\sigma^x\rangle = 0$). Standard observables such as correlation functions or excited states energies are easy to obtain since a Jordan-Wigner transformation maps this model onto a free-fermion Hamiltonian. The EE is also easily accessible using the free particle/Gaussian description of reduced density matrices [56]. However, contrary to TL liquids, we have few analytical results concerning the SRE of this system and our understanding of the SRE is mostly based on numerical observations. The SRE gives a striking example of a simply-defined universal quantity which has, so far, escaped any field theory treatment. The critical value of the Rényi parameter appears to be $n_c = 1$ for the critical Ising model and moving away from $n = 1$ – above or below – seems to play the role of a relevant perturbation. This contrasts with TL liquids, which belong to a line a fixed points, and where the parameter n could be used to move along this line.

There are two natural basis choices to compute the SRE: the σ^z basis, and the σ^x one. However, the Kramers-Wannier duality can be used to exchange the role of σ^z and σ^x and to show that the SRE S_n^x computed in the x basis is simply related to that in the z basis: $S_n^x(\mu) = S_n^z(1/\mu) + \log(2)$ [2]. The extensive part is thus the same in the two basis, while the subleading terms differ by $\log(2)$. To avoid any confusion we restrict here to the x basis, which also corresponds to spin configurations in the classical 2D point of view. We will comment at the end on the possibility to interpolate between the x and z directions.

The data were obtained by summation over 2^L configurations up to $L = 44$ [4]. Thanks to the free fermion formulation, each probability p_i can be written as the determinant of an $L \times L$ matrix which entries depend on the spin configuration $|i\rangle$.[14]

As in all the cases discussed so far the SRE of the ICTF has a leading term proportional to L (visible in Fig. 2.5), and a subleading correction of $\mathcal{O}(1)$ (for periodic chains) which is noted $r_n(\mu)$, where μ is the coupling strength (Eq. 2.26) and n is the Rényi parameter.

2.2.1 Numerics at $n = 1$

Ordered and disordered phases

The Shannon entropy is very simple when $\mu \to \infty$, since the finite-size ground state simply becomes $\frac{1}{\sqrt{2}}(|\uparrow\cdots\uparrow\rangle + |\downarrow\cdots\downarrow\rangle)$. The entropy is not extensive in this limit and we are left with a subleading term $r_1(\mu \to \infty) = \log(2)$. Doing a first-order expansion in $1/\mu$ will dress each of the two components of the ground state by spin flips (application of σ^z). Such corrections will produce an extensive term in the entropy, but it can easily be checked that they will not affect the subleading term. We can also invoke the universality of the subleading entropy constant to argue that $r_1(\mu)$ should be constant in the whole phase. The data of the left panel of Fig. 2.6 are indeed consistent with $r_1 = \log(2)$ in the ordered phase, even if finite-size effects (oscillations) are important. For a general gapped phase with spontaneously broken symmetry we expect the subleading term in the SRE to be $\log(\text{deg})$, where deg is the degeneracy. This has been checked, for instance, for the XXZ chain in the gapped phase ($\Delta > 1$) [2], and in some 2D systems as well [54].

[14] The largest chain requires to sum $2^{44} \simeq 17.10^{12}$ determinants of size 44×44. It was possible to do so in a reasonable amount of time thanks to some (trivial) parallelization, as well as thanks to an algorithm which generates "bracelets" [127]. The later produces one representative configuration for each orbit of spin configurations related by lattice symmetries (translations and inversion), together with its multiplicity. Importantly, the method works without the need to *store* the configurations. The free fermion formalism gives an easy access to probabilities in the σ^z basis. The entropy in the other basis is then obtained by duality.

The same arguments work in the disordered phase, where the $\mu = 0$ limit gives an entropy equal to $L \log(2)$, with a vanishing subleading constant. Again, we expect $r_1(\mu)$ to vanish in the whole $|\mu| < 1$ phase.

Critical point

The most interesting results are those at (or in the vicinity) of the critical point at $\mu = 1$. The SRE of the critical ICTF is plotted in Fig. 2.5 (crosses) and the relatively long chains allowed to determine the subleading constant (noted r_1 in Fig. 2.6) with high accuracy:[15]

$$r_1 = 0.2543925(5). \tag{2.27}$$

Of course, this number is interesting only if it is universal... We expect on general grounds these subleading entropy constants to be universal, but it is nevertheless useful to check it explicitly. To this end we considered two other different microscopic realizations of the Ising universality class: the ferromagnetic Ising model on the triangular lattice, and the Ising model on the square lattice (both at $T = T_c$). In those two other cases the probabilities were obtained by diagonalizing numerically the classical transfer matrix. In these two cases the entropy is exactly the Shannon entropy of a line of spins in the bulk of a classical 2D Ising model. The data are shown in Fig. 2.5 (triangles and squares). Although the systems sizes are smaller than for the ICTF, these two systems indicate the presence of a subleading $r_1 \simeq 0.254$, consistent with the value found for the ICTF (see [106] for data on larger square lattices).

2.2.2 Numerics for $n \neq 1$

As for the compactified boson case, some insight can be gained on the subleading entropy constant if one varies the Rényi parameter. Here μ is thus fixed to 1 and n is varied. The data for $r_n(\mu = 1)$ are presented in the right panel of Fig. 2.6. We observe that the subleading entropy constant goes from 0 to $\log(2)$ when n increases, with some "crossing" at $n = 1$. Thanks to exact results at $n = \frac{1}{2}$ and $n = \infty$, the two limiting values are relatively easy to understand.

Large n phase

The limit $n = \infty$ is relatively simple since it amounts to compute the highest probability $p_{\max}$, which is that of a fully polarized spin configuration in the x direction. If we consider the ICTF ground state as the dominant eigenvector of the transfer matrix of some 2D classical Ising model, $p_{\max}$ is the ratio $(\mathcal{Z}_{\text{fixed}})^2/\mathcal{Z}$, where the partition function $\mathcal{Z}_{\text{fixed}}$ is that of a semi-infinite cylinder with a ferromagnetic condition at its boundary, and $\mathcal{Z}$ has no boundary (infinite cylinder). The ferromagnetic condition on the spins corresponds (or "flows") to a conformally invariant boundary state in the continuous limit, usually noted "+" (or "fixed"). The universal piece of the above partition ratio is the square of associated g-factor (as in Eq. 2.14). The later was shown by Cardy [128, 129] to be $g_+ = \frac{1}{\sqrt{2}}$, which gives a subleading

[15] Our data have been re-analyzed by Lau and Grassberger [106], leading to a slightly higher accuracy: $r_1 = 0.254392505(10)$. There are probably few examples in statistical physics of universal numbers associated to phase transitions which are known numerically with such an accuracy and we are yet to be understood theoretically.

term $\log(2)$ to $-\log p_{\max} = S_{n=\infty}$ (see [2] for more details).[16] Our numerical data indicate that the subleading term in the SRE is $\log(2)$ for $n \gtrsim 1.5$, and probably also for any $n > 1$. Still, based on the available system sizes, one cannot exclude some smooth function of n which would reach $\log(2)$ at some new critical $n \in]1, \simeq 1.5]$. Nevertheless, the inset of the right panel of Fig. 2.6 suggests that the slope $\frac{\partial r_n}{\partial n}\big|_{n=1,\mu=1}$ could slowly diverges with the system size, typically as $\sim L^{0.25}$. A plausible scenario is therefore $r_{n>1}(\mu = 1) = \log 2$ in the thermodynamic limit.

As in Sec. 2.1.2, if $2n$ is an integer, the sum $\mathcal{Z}(n) = \sum_i p_i^n$ can be interpreted as the partition function of a book. If r_n is indeed discontinuous at $n = 1$ in the thermodynamic limit it would indicate that the binding of that book flows to a "fixed" boundary condition (and decoupled sheets) for $n > 1$. We may thus say that taking n away from 1 is a relevant perturbation for the book binding. At $n = 1$ the binding is just a line in the bulk of the cylinder. However, as soon as $n \neq 1$ the binding becomes a special line, with correlations that are different from the bulk ones.[17] The SRE problem in the vicinity of $n = 1$ might be related to line defects in the 2D Ising model, but it is unclear to us how the results of Oshikawa and Affleck [130] can be applied to understand, for instance, Eq. 2.27.

We finally mention that the SRE of the quantum Ising model in two spatial dimensions was recently investigated using QMC [54], with several interesting findings concerning new universal subleading entropy constants for $n = 2, 3$ and ∞.

Small n phase

To understand what happens for $n < 1$ it is useful to consider the case $n = \frac{1}{2}$. This value of the Rényi parameter plays a special role since $\sqrt{p_i} = \langle \psi | \, i \rangle$ is *linear* in the coefficients of the ground state wave function $|\psi\rangle$.[18] The partition function of the single-sheet book $\mathcal{Z}(\frac{1}{2}) = \sum_i \langle \psi | \, i \rangle = \langle \psi | \sum_i |i\rangle$ is the scalar product between $|\psi\rangle$ and the equal amplitude superposition of all the Ising configurations (x basis). The later is nothing but a polarized state in the z direction,

$$|\text{free}\rangle = |{\rightarrow_z} \cdots {\rightarrow_z}\rangle = \frac{1}{2^{L/2}} \sum_{\sigma_i^x = \pm} |\sigma_1^x \cdots \sigma_1^x\rangle \,, \tag{2.28}$$

so that we can write

$$\mathcal{Z}\left(\frac{1}{2}\right) = 2^{L/2} \, \langle \psi \, | \text{free} \rangle \,. \tag{2.29}$$

Since $|\text{free}\rangle$ is the vacuum of the Jordan-Wigner fermions, the scalar product above can be computed exactly [2]:

$$\langle \psi | \text{free} \rangle = \prod_{j=0}^{L/2-1} \cos \frac{(2j+1)\pi}{4L}. \tag{2.30}$$

[16] $p_{\max}$ can also be obtained exactly on the lattice by first computing the probability of the ferromagnetic configuration in the z basis (fermion vacuum), and then using the Kramers-Wannier duality.

[17] Spin-spin correlations were recently investigated as a function of n [112] and were found to be long-range ordered for $n \gtrsim 1.5$. Finite-size effects are however still too large to conclude whether correlations are long-ranged or algebraic in the interval $n \in]1, 1.5[$.

[18] ψ_i can be chosen real and positive (Perron-Frobenius theorem).

And an Euler-Maclaurin expansion (for large L) can finally be used to show the $\mathcal{O}(1)$ term in the SRE vanishes [2, 4]:

$$S_{\frac{1}{2}}(\mu = 1) = 2\log \mathcal{Z}\left(\frac{1}{2}\right) = \frac{2K}{\pi}L + o(1) \tag{2.31}$$

$$K \simeq 0.91596559 \text{ (Catalan's constant)}. \tag{2.32}$$

As for the $n = \infty$ limit, the vanishing of $r_{\frac{1}{2}}$ can also be obtained by remarking that $\mathcal{Z}(\frac{1}{2})$ is an Ising model partition function on a half-infinite cylinder with a free boundary condition. The universal piece of this partition function is again some g-factor associated to a well-known conformal boundary state, for which $g_{\text{free}} = 1$.

From our numerical calculations it is clear that r_n vanishes for $n \lesssim 1/2$ but it also seems likely that $r_n = 0$ in the whole interval $[0, 1[$, although the convergence to the thermodynamic limit is quite slow. The boundary is known to be critical at $n = \frac{1}{2}$ and it is probably the case for all $n < 1$, although finding numerically the exponent is difficult [112].

2.2.3 Geometrical entanglement and basis rotations

We wish to conclude this chapter by mentioning a related application of these boundary states ideas. The *geometric entanglement* (GE) (see [131] and references therein) is defined by taking a state $|\psi\rangle$ and looking for the closest *separable* state $|S\rangle$ in the Hilbert space. The GE entanglement is then $\mathcal{E} = -\log\left(|\langle S\,|\psi\rangle|^2\right)$ and vanishes if and only if $|\psi\rangle$ is separable. One interesting property of this quantity in the context of condensed matter problems is that it can be used in simulations to detect phase transitions. For a spin chain, the natural definition of "separable" is a product of single-spin states.

For the critical ICTF the product state which maximizes the overlap with the ground state is a tilted configuration [132]:

$$|S\rangle = \bigotimes_{i=1}^{L} (\cos(\xi/2)|\uparrow_i\rangle + \sin(\xi/2)|\downarrow_i\rangle) \tag{2.33}$$

where $|\uparrow_i\rangle$ and $|\downarrow_i\rangle$ are the eigenstates of σ_i^z and the optimal angle ξ is $\simeq 0.897101$ (non-universal).

The scalar product $\langle S\,|\psi\rangle$ can be interpreted as a boundary contribution to the free energy of a classical 2D Ising model. If we had to project $|\psi\rangle$ onto a state where all the spins would point in the x direction (corresponding to an angle $\xi = \pm\pi$), it would be a fixed ferromagnetic boundary condition for the Ising model. On the other hand, projecting onto a state with all the spins pointing in the z direction ($\xi = 0$) would correspond to the $|\text{free}\rangle$ condition. The tilted state of Eq. 2.33 then appears to be intermediate between free and fixed boundary conditions. The important point is however that $\xi \neq 0$, which means that $|S\rangle$ breaks the $\mathbb{Z}_2$ symmetry of the model ($\sigma^x \leftrightarrow -\sigma^x$). In such situation where the boundary condition imposes a non-zero magnetization at the edge, the long-distance and universal properties of the boundary will be equivalent to that of a system with fixed ferromagnetic boundary condition "+" (all spins pointing in the x direction) [93]. This is due to the attractiveness of the "fixed" boundary state under the RG flow. We thus find [3] that $\mathcal{E}$ contains a subleading term equal to $-\log(g_+^2) = \log(2)$, as conjectured in Ref. [133].

The scalar product between the ICTF ground state and $|S\rangle$ can alternatively be viewed as the $p_{\max}$ computed in a rotated basis, it is thus related to $S_{n=\infty}$ in that new basis. But, more

interestingly, the subleading entropy constant at $n = 1$ ($\simeq 0.254$, Eq. 2.27) was also observed to be independent of global basis rotations[19] [J.-M. Stéphan, unpublished]. From these two examples (at $n = 1$ and $n = \infty$) we can conjecture that universal entropy constants should be robust, at least to some extent, to basis rotations.

We finally mention that similar ideas have been applied to compute the subleading term in the GE of the critical XXZ chain [3].

[19] As long as the rotated basis has some component along the x axis.

Chapter 3

Shannon-Rényi entropy for Nambu-Goldstone modes in dimension two

We are here interested in 2D quantum spin systems where the spin rotation symmetry – $U(1)$ or $SU(2)$ for instance – is broken at zero temperature. In such systems with magnetic long-range order and gapless Nambu-Goldstone modes, it was observed, using (modified) spin-wave calculations [134] and QMC on Heisenberg models [135] that the *entanglement* entropy possesses some additive $\log L$ corrections to the boundary law. Soon after, these results were explained by some analytical calculations (quantum rotor model and a non-linear sigma model) [45], leading to the prediction that the coefficient of $\log L$ is $N_{\rm NG}/2$, where $N_{\rm NG}$ is the number of Nambu-Goldstone modes.

Very recently, the SRE of several 2D magnets were computed using QMC [54, 136, 114]. By simulating spin-$\frac{1}{2}$ XXZ and Heisenberg models, $U(1)$ and $SU(2)$ broken symmetries were investigated. The SRE for the complete system (torus), as well as the entropy of a line subsystem were measured. In all theses cases, as summarized in Tab. 3.1, some additive $\log L$ corrections have been observed.

These results motivated us to look for a field-theory description of these logarithmic contributions, somewhat in the spirit of [45] for the EE. The calculations presented below is based on some unpublished work done in collaboration with Masaki Oshikawa and Vincent Pasquier, and which also benefited a lot from discussions with Fabien Alet and Nicolas Laflorencie.

3.1 Oscillator/spin-wave contributions

3.1.1 Massless free scalar field

We first assume that the system is in a broken symmetry state, with a well defined direction of the order parameter (say x). At low energy the interactions between spin-waves are irrelevant and each mode can be described by a free gapless scalar boson with a linear dispersion relation. As consequence we can consider the case of a single mode (broken $U(1)$), and multiply the final result by the number of Nambu-Goldstone modes.

At each point $\mathbf{r}$ in space an angle $\phi_{\mathbf{r}}$ describes the local orientation of the order parameter with respect to its average direction. At low energies and when coarse grained over sufficiently

Model	n	$\log(N)$ coef. Ref. [54]	$\frac{N_{\rm NG}}{4}\frac{n+1}{n-1}$	Model	n	$\log(N)$ coef. Ref. [54]	$\frac{N_{\rm NG}}{4}\frac{n+1}{n-1}$
Heisenberg				XY			
$J_2=0$	∞	0.460(5)	0.5	$J_2=0$	∞	0.281(8)	0.25
$J_2=-5$	∞	0.58(2)	0.5	$J_2=-1$	∞	0.282(3)	0.25
$J_2=0$	2	1.0(2)	1.5	$J_2=0$	2	0.585(6)	0.75
$J_2=-5$	2	1.25(4)	1.5	$J_2=-1$	2	0.598(4)	0.75
				$J_2=0$	3	0.44(2)	0.5
$J_2=-5$	3	1.06(3)	1	$J_2=-1$	3	0.432(7)	0.5
				$J_2=0$	4	0.35(8)	0.4166
$J_2=-5$	4	1.0(1)	0.8333	$J_2=-1$	4	0.38(2)	0.4166

Table 3.1: Subleading logarithmic terms in the SRE of the 2D Heisenberg and XY models, possibly with ferromagnetic second neighbor interaction J_2 (which strengthens the magnetic order). n is the Rényi (noted q in [54]). The numerical values obtained by Toulouse's group (supplementary material of [54]) are given in the third column. We selected the best fit only for simplicity – which does not do justice to their extensive and detailed data analysis. The last column is the present theoretical prediction (Eq. 3.24), which combines the oscillators (Eq. 3.10) and TOS contributions (Eq. 3.23). The number $N_{\rm NG}$ of Nambu-Goldstone mode is 2 for Heisenberg and 1 for XY.

long distances, these deviations are small and one can treat them as real numbers, therefore neglecting the compactness of $\phi_{\mathbf{r}}$. This leads to the Hamiltonian of a massless free scalar field:

$$H = \frac{1}{2}\int d^2\mathbf{r}\left[\chi_\perp \Pi_{\mathbf{r}}^2 + \rho_s\left(\nabla\phi_{\mathbf{r}}\right)^2\right] \tag{3.1}$$

where ρ_s is the stiffness, $\chi_\perp = \frac{c^2}{\rho_s}$ is the transverse susceptibility, c the spin-wave velocity, and $\Pi_{\mathbf{r}} = \frac{\rho_s}{c^2}\dot{\phi}_{\mathbf{r}}$ is canonically conjugate to $\phi_{\mathbf{r}}$. This is a collection of harmonic oscillators, one for each momentum $\mathbf{k}$:

$$H = \frac{1}{2}\sum_{\mathbf{k}}\left[\frac{c^2}{\rho_s}\Pi_{\mathbf{k}}^2 + \rho_s\mathbf{k}^2\left|\phi_{\mathbf{k}}\right|\right]. \tag{3.2}$$

3.1.2 Configuration with the highest probability

We start by considering the $n=\infty$ SRE, which amounts to evaluate the probability of the most likely configuration.

Let us first recall that the (normalized) ground state wave function ψ of an harmonic oscillator with the Hamiltonian $H = \frac{1}{2m}p^2 + \frac{1}{2}m\omega^2x^2$ is

$$\psi(x) = \left(\frac{m\omega}{\pi}\right)^{1/4}\exp\left(-\frac{m\omega}{2}x^2\right). \tag{3.3}$$

So, if one asks what is the probability density $p_{\max}$ to find the particle at its "most likely" location, the result is the square of the wave function at $x=0$, which is just the square of the normalization factor :

$$p_{\max} = |\psi(0)|^2 = \left(\frac{m\omega}{\pi}\right)^{1/2}. \tag{3.4}$$

Comparing this to Eq. 3.2, the mode $\mathbf{k}$ of the free field has a mass $m_{\mathbf{k}} = \frac{\rho_s}{c^2}$ and frequency $\omega_{\mathbf{k}} = c|\mathbf{k}|$. So, the probability $p_{\max}(\mathbf{k})$ for the mode $\mathbf{k}$ to be "at the origin" is:

$$p_{\max}(\mathbf{k}) = \left(\frac{m_{\mathbf{k}}\omega_{\mathbf{k}}}{\pi}\right)^{1/2} = \left(\frac{\rho_s|\mathbf{k}|}{\pi c}\right)^{1/2}. \tag{3.5}$$

We are interested in the probability density to observe $\phi_{\mathbf{r}} = 0$ everywhere in space, so we impose $\phi_{\mathbf{k}} = 0$ for all $\mathbf{k}$ and get:

$$p_{\max}^{\text{osc}} = \prod_{\mathbf{k}\neq 0} p_{\max}(\mathbf{k}) = \prod_{\mathbf{k}\neq 0}\left(\frac{\rho_s|\mathbf{k}|}{\pi c}\right)^{1/2}. \tag{3.6}$$

Taking the logarithm we obtain:

$$-\log\left(p_{\max}^{\text{osc}}\right) \quad = \quad -\frac{1}{2}\sum_{\mathbf{k}\neq 0}\log\left(\frac{\rho_s}{\pi c}\right) - \frac{1}{4}\sum_{\mathbf{k}\neq 0}\log\left(\mathbf{k}^2\right). \tag{3.7}$$

The zero mode $\mathbf{k} = 0$ is omitted since we assume that the system is in a broken-symmetry state. Including the zero mode would, in a finite volume, "delocalize" the order parameter and restore the rotation symmetry. We will take later into account the rotational symmetry of the finite-size ground state by a correcting factor associated with the "degeneracy" of the Anderson tower of states (TOS), see Sec. 3.2. The first sum is simply a volume term ($\sim L^2$) but the universal contribution comes from the second sum, which we analyze now.

3.1.3 Determinant of Laplacian

Since the $-\mathbf{k}^2$ are the eigenvalues of the Laplacian Δ, the Eq. 3.7 is a lattice regularization of $\log\det'\Delta$, where $\det'$ means that the zero eigenvalue is removed. One can regularize the sum by using a periodic $L\times L$ lattice (torus), in which case the universal terms in the $L\to\infty$ asymptotics can be extracted by means of an Euler-Maclaurin expansion.[1] But $\det'\Delta$ is in fact a quantity which has been studied a lot (see for instance [100, 137]). In particular:

$$\log\det{}'\,\Delta \simeq \mathcal{O}(L^2) + \left(1-\frac{\chi}{6}\right)\log\left(\mathrm{L}^2\right), \tag{3.8}$$

where χ is the Euler characteristics of the manifold. This result is remarkable since the coefficient of the $\log(L^2)$ term is purely topological. It can be derived using the heat-kernel method and zeta regularization for instance [138]. We therefore have:

$$-\log(p_{\max}^{\text{osc}}) = \mathcal{O}(L^2) + \frac{1}{4}\left(\frac{\chi}{6}-1\right)\log\left(L^2\right) + \mathcal{O}(1). \tag{3.9}$$

And, specializing to the torus ($\chi = 0$):

$$-\log(p_{\max}^{\text{osc}}) = \mathcal{O}(L^2) - \frac{1}{4}\log\left(L^2\right) + \mathcal{O}(1). \tag{3.10}$$

[1] A possible regularization is to use the Brillouin zone of an $L\times L$ square lattice : $\Sigma(L) = \sum_{\mathbf{k}\neq 0}\log\left(\mathbf{k}^2\right) = \sum'_{n,m=-\frac{L}{2}\cdots\frac{L}{2}-1}\log\left(k_n^2+k_m^2\right)$ where the discrete momenta are given by $k_n = \frac{2\pi n}{L}$ and the zero-mode ($n = m = 0$) is omitted. Using twice the Euler-Maclaurin expansion at the trapezoid order gives: $\Sigma(L) = \left(\frac{1}{2}\pi - 3 - \log(2) + 2\log(2\pi)\right)L^2 + \log\left(L^2\right) + \mathcal{O}(1)$. While the term proportional to L^2 depends on the regularization scheme, the $\log\left(L^2\right)$ is universal.

If compared with the numerical QMC results for the $n = \infty$ SRE (Tab. 3.1), the log coefficient $-\frac{N_{\rm NG}}{4}$ obtained above is clearly off, with a wrong sign in particular. As we argue below, this is due to the fact that the oscillator contribution provides only one part of the logarithmic terms. The other part, discussed in Sec. 3.2, is due to the fact that the ground state of a system of finite volume is rotationally invariant, contrary to the initial assumption of a broken-symmetry state. But before dealing with this important point, we comment on the n dependence of the oscillator contribution to the SRE.

3.1.4 Rényi index and Gaussian probabilities

So far we only considered one probability, $p_{\rm max}$, of observing the configuration with $\phi_{\mathbf{r}} = 0$ everywhere. Here we show that, for Gaussian variables, the universal part of SRE

$$S_n^{\rm osc} = \frac{1}{1-n} \log \sum_{\{\phi_{\mathbf{r}}\}} (p_\phi)^n \tag{3.11}$$

can be obtained from $p_{\rm max}$ alone. The argument is almost identical to that of Sec. 2.1.2, and we do not repeat it in details. Here p_ϕ refers to the probability of a configuration $\{\phi_{\mathbf{r}}\}$, defined on the whole system (or in a subsystem). If the field configurations are distributed in a Gaussian way we can write these probabilities as:

$$p(\phi)_{\rho_s} = p(\phi = 0)_{\rho_s} \exp\left(-\frac{1}{2}\rho_s \phi \cdot G^{-1} \cdot \phi\right) \tag{3.12}$$

$$= p_{{\rm max},\rho_s} \exp\left(-\frac{1}{2}\rho_s \phi \cdot G^{-1} \cdot \phi\right), \tag{3.13}$$

where G is the propagator and we explicitly keep the stiffness ρ_s. Repeating the manipulations of Sec. 2.1.2 leads to

$$S_n^{\rm osc} = \frac{1}{n-1} \left[\log\left(p_{{\rm max},n\rho_s}\right) - n \log\left(p_{{\rm max},\rho_s}\right)\right]. \tag{3.14}$$

For the massless oscillators discussed previously, the universal logarithm turned out to be independent of the stiffness ρ_s (see Eq. 3.10). So, $\log\left(p_{{\rm max},n\rho_s}\right)$ and $\log\left(p_{{\rm max},\rho_s}\right)$ have the same subleading logarithms and we may thus write:

$$S_n^{\rm osc} \underset{\log(L)\text{ terms}}{=} -\log\left(p_{\rm max}^{\rm osc}\right) \tag{3.15}$$

which is independent of the Rényi index n. Naturally this only holds as long as the non-Gaussian effects can be neglected, which is presumably correct for small enough n, including $n = 1$ (and also, obviously, at $n = \infty$).

As in 1+1D, we note that there may be a critical value of n beyond which the probabilities $(p_\phi)^n$ would no longer describe a gapless system, but a gapped state. Indeed, the choice of a basis to compute the entropies was made by selecting one particular spin direction in the ordering plane. For $n > 1$ such a choice explicitly breaks the $U(1)$ symmetry down to $\mathbb{Z}_2$. Increasing n favors the spin configurations which are polarized along (or exactly opposite to) the quantization axis of the basis. So, we may expect that, beyond some critical n_c, the state $|\psi, n\rangle$ would have some Ising-like long-range order and a finite correlation length. Investigating this question further (numerically and/or analytically) would clearly be an interesting direction of research.

3.2 Degeneracy factor

3.2.1 Tower of states

Let us briefly review the (standard) concept of tower of states (TOS) [139, 140, 141], which reconcile the fact that the finite-size (antiferromagnetic) eigenstates are rotationally invariant while, in $D \geq 2$, the system can break the rotational symmetry in the infinite volume limit at $T = 0$.

If a spin Hamiltonian $\mathcal{H}$ has a continuous rotation symmetry, say $U(1)$ for simplicity, the total angular momentum $S^z_{\text{tot}} = \sum_{\mathbf{r}} S^z_{\mathbf{r}}$ (generator of the rotations) is a conserved quantity, and one can chose the eigenstates of $\mathcal{H}$ such that they are also eigenstates of S^z_{tot}. For an antiferromagnetic system, the finite-size ground state has $S^z_{\text{tot}} = 0$ and is thus rotationally invariant.[2] But the energy spectrum also has a set of low-energy eigenstates, with all values of S^z_{tot} up to $\sim \sqrt{N}$. They form the so-called Anderson TOS and their energies scale as $E \simeq E_0 + \frac{1}{N\chi} (S^z_{\text{tot}})^2$, where N is the number of sites and χ the uniform susceptibility along the z axis. Their energy is at most $\sim \mathcal{O}(1)$ above the absolute ground state and their uniform magnetization per site, measured along the z axis, is small but non-zero : at most $\sim N^{-\frac{1}{2}}$.

A symmetry-breaking state can be constructed by a linear combination of the eigenstates of the tower. Due to the slight energy differences between the eigenstates of the TOS, a symmetry-breaking combination is no longer an exact eigenstate, but it is a low-energy state. The dimension of the TOS is not defined exactly, but should be understood in the scaling sense. In the $U(1)$ case the highest angular momenta scale as $\sim \sqrt{N}$ and the dimension of the TOS is $\sim \sqrt{N}$.[3]

As a basic consequence of uncertainty relations, the more localized is the direction of the order parameter on the unit circle (in the xy plane), the higher are the S^z_{tot} fluctuations. Because a low-energy symmetry-breaking state is built from states in the TOS, which has some "cut off" $\sim \sqrt{N}$ on S^z_{tot}, the order parameter direction can be at best defined with an angular precision $\delta\theta \sim 2\pi N^{-\frac{1}{2}}$. In other words, a low-energy symmetry-breaking state "occupies" a finite patch on the circle representing all the possible order parameter directions. The same argument, when applied to an $SU(2)$ symmetry broken down to $U(1)$ (collinear antiferromagnet) leads to the conclusion that a low-energy symmetry-breaking state occupies a solid angle $\delta\Omega \sim 4\pi N^{-1}$ on the Bloch sphere representing the order parameter manifold.

In a more general situation we expect (phase space volume argument) the TOS dimension Q to scale as $\sim N^\alpha$, with an exponent α which only depends on the number of Nambu-Goldstone modes:

$$\alpha = N_{\text{NG}}/2. \tag{3.16}$$

3.2.2 Symmetric ground state and $p_{\max}$

For the entropy problem at hand, we propose to adopt the dual point of view, where the symmetric finite-size ground state $|\Psi\rangle$, with $S^z_{\text{tot}} = 0$, is built as a linear superposition of

[2] This was shown rigorously for an Heisenberg-like (or XXZ) model on a bipartite lattice (with the same number of sites on both sublattices): the Lieb-Mattis theorem [142].

[3] If, instead, the Hamiltonian symmetry is $SU(2)$ and it is broken down to a residual $U(1)$, the relevant quantum number is the total spin $\left(\vec{S}_{\text{tot}}\right)^2 = S(S+1)$. In that case the maximal total spin in the TOS scales as $S \sim \sqrt{N}$. Due to the additional Zeeman degeneracy compared to $U(1)$, the TOS has a larger dimension, which scales as $\sim N$.

$Q \sim N^\alpha$ symmetry-breaking states noted $\{|1\rangle, |2\rangle, \cdots, |Q\rangle\}$. The $U(1)$ case would correspond to $\alpha = \frac{1}{2}$ and $SU(2) \to U(1)$ would be $\alpha = 1$. We thus write:

$$|\Psi\rangle = \frac{1}{\sqrt{Q}} \left(|1\rangle + |2\rangle + \cdots + |Q\rangle\right). \tag{3.17}$$

Now we wish to compute the probability of a perfectly ordered spin configuration, noted $|+\rangle$:

$$p_{\max} = |\langle\Psi|+\rangle|^2 = \frac{1}{Q}\left|\sum_{i=1}^{Q}\langle i\,|+\rangle\right|^2. \tag{3.18}$$

We can choose the states appearing in Eq. 3.17 so that only one, say $|1\rangle$, has an order parameter direction which matches that of the classical configuration $|+\rangle$. We argue that $\sum_{i=1}^{Q}\langle i|+\rangle$ is dominated by the $i = 1$ term and that the others may be ignored when $N \to \infty$. This approximation should only alter the extensive part of $-\log p_{\max}$. The idea is that the scalar product of a symmetry breaking state $|i \neq 1\rangle$ with $|+\rangle$ (which points in a different direction) is purely exponential, and insensitive to the presence of long wavelength fluctuations in $|i\rangle$. On the other hand, since the state $|1\rangle$ is "aligned" with the classical state $|+\rangle$, $\langle 1|+\rangle$ will precisely have the oscillator contribution discussed in Sec. 3.1. So, as far as the universal part is concerned, we may write

$$p_{\max} \simeq \frac{1}{Q}\,|\langle 1|+\rangle|^2 \tag{3.19}$$

with $Q \sim N^{N_{\rm NG}/2}$. We finally get:

$$-\log\left(p_{\max}\right) \simeq -\log\left(p_{\max}^{\rm osc}\right) + \frac{1}{2}N_{\rm NG}\log(N) \tag{3.20}$$

$$\simeq +\frac{1}{4}N_{\rm NG}\log(N), \tag{3.21}$$

which, from Tab. 3.1, appears to be in *reasonable* agreement with the QMC data of Luitz *et al.* [54] at $n = \infty$. We also note that their results for models *without* continuous symmetry breaking (gapped phase of the XXZ model) indicate the absence of log correction, which is of course consistent with the present analysis. We will now attempt to describe the log corrections in the finite-n SRE.

3.2.3 Dependence with n

We have introduced a degeneracy factor $Q \sim N^\alpha$ to describe how $p_{\max}$ is modified by the rotational symmetry of the finite-size ground state (compared to that of a broken-symmetry state). We now assume further that the same factor applies to all the probabilities: $p(\phi) = \frac{1}{Q}p(\phi)^{\rm osc}$. Although difficult to justify rigorously, it is a plausible assumption for the configurations ϕ which are close to $\phi = 0$, and thus plausible for the "large" probabilities, which are the relevant ones when n is not too small. The factor $1/Q$ in front of each probability contributes to the SRE by

$$S_n^{\rm TOS} = \frac{n}{n-1}\log(Q) = \alpha\frac{n}{n-1}\log(N). \tag{3.22}$$

As an important check of the equation above we note that it is in agreement with the exact result for the logarithmic term in SRE of the Lieb-Mattis model [54], which has an $SU(2) \to$

$U(1)$ TOS [hence $\alpha = 1$] but no gapless spin-waves ($\rightarrow$ no oscillator contribution to the entropy).

Next we add the oscillator part, and since $S_n^{\rm osc}$ is independent of n (Eq. 3.15) we get:

$$S_n \underset{\log(L)\text{ terms}}{=} \frac{n}{n-1}\log(Q) - \log\left(p_{\rm max}^{\rm osc}\right). \tag{3.23}$$

Replacing Q by $N^{N_{\rm NG}/2}$ and $-\log\left(p_{\rm max}^{\rm osc}\right)$ by Eq. 3.10 we finally obtain:

$$S_n \underset{\log(N)\text{ terms}}{=} \frac{N_{\rm NG}}{4}\frac{n+1}{n-1}\log(N). \tag{3.24}$$

In Tab. 3.1 the result above is compared to the QMC results obtained by Toulouse's group, for $n = 2, 3$ and 4. The agreement is not excellent, and somewhat worse for finite n than for $n = \infty$. We believe that the present approach may still be correct, even though we are clearly still far from a controlled calculation. In particular, while our treatment of the TOS seems justified for $p_{\rm max}$, it is perhaps too crude at finite n. Finally, we note that when n increases, the Rényified state may experience a phase transition, and Eq. 3.24 would no longer be valid beyond n_c. Since strong finite-size effects have been observed in the vicinity of such transitions in 1D (see in particular Fig. 2.4), a similar difficulty could be present here too (note also that the error bars given in Tab. 3.1 do not include the variations when larger system sizes are included). We do not have any concrete indication of a transition, but it could take place in the range of values of n that have been studied in QMC. In any case, it would be interesting to look for possible signatures of such a transition in the simulations.

Conclusion

The works summarized in this manuscript were initially motivated by some questions about EE and ES. We started with rather specific (toy) wave functions, the constrained RK states, and realized that the RDMs in these states have a very simple structure, and that the eigenvalues of these RDM can be obtained easily. Exploiting this observation, we could check numerically with precision several earlier theoretical predictions: the possibility to extract the TEE in a lattice model, its value log(2) in a dimer liquid with finite correlation length, its independence from the Rényi index [1, 6], or the presence of logarithmic corrections to the EE when the subsystem has some sharp corners [111, 5, 117].

On the way we were lead to consider some different information-related quantities to probe a many-body wave function, the Shannon-Rényi entropies. It is probably in that direction that our work will have the greatest number of interesting extensions. These SRE have already been recognized as interesting and useful and they are now being studied by several other groups [117, 106, 108, 118, 54]. So, we would like to conclude this manuscript by listing some problems and directions, related to SRE, which seem worth exploring further.

One can argue against the general interest of SRE because these entropies are basis dependent – which is true.[4] We nevertheless showed that, in some appropriate basis, the SRE contains some universal information about the phases: degeneracy in gapped phases with discrete broken symmetry, compactification radius in a TL liquid, or number of Nambu-Goldstone in 2D. In some specific cases we saw that the universal terms are robust to some rotation of the basis states, but it still remains to understand to which extend the universal terms in the SRE depends on the basis.

It would be desirable to develop some field theory method which could deal with partition functions on "books", and, more difficult, partition functions of their continuous-n versions. We need to understand better in which situations the SRE entropy can be tackled using existing (boundary) CFT tools, and when it cannot. The problem could essentially be solved for the Gaussian free field, but it remains unsolved in general. The cases $n = \frac{1}{2}$ and $n = \infty$ are relatively simple to treat, because they are related to single-sheet partition functions, but understanding the behavior at $n = n_c$ is clearly more demanding. In the Ising model for instance, determining the mysterious constant of Eq. 2.27 seems to require to understand how to treat a perturbation corresponding to $n = 1 + \epsilon$.

We have mostly discussed here the SRE of a complete system, in 1 or 2D. But the partial SRE of a subsystem[5] is another interesting quantity, with some striking analogies to the entanglement entropy. A segment in a critical chain [111, 118, 112] and a line in a 2D [114] are the only cases which have been looked at so far. It is however likely that some other

[4] One would however not argue against the interest of spin-spin correlations simply because they depend on the spin direction ($\langle S^x_0 S^x_r \rangle$ is generally not the same as $\langle S^x_0 S^x_r \rangle$).

[5] Or, more precisely, the mutual information.

universal contributions will be observed in other phases and other geometries. As an example, can we detect some discrete symmetry breaking, topological order or many-body localization using partial SRE ? Along the same line, understanding the structure of the probabilities in a subsystem (that is the diagonal part of the reduced density matrix), as was initiated in [114], seems to be a promising way to look at many-body states.

The *Rényified* states, that we note $|\psi, n\rangle$ (Eq. 2.2), are deformations of a given wave function. In a suitable basis, increasing n is a way to enhance the weights of ordered configuration(s) until the point where the state becomes long-range ordered. Apart from a few results on the XXZ chain, and the results for the ICTF [112], there has been relatively few calculations concerning correlations in such deformed states. We however note that the QMC algorithm or Ref. [54] is, in principle, able to compute some correlation functions in a Rényified state (for integer n, not too large). Since it is often very useful to introduce some additional "axis" in the phase diagram to identify possible instabilities and competing phases, the Rényi index should also be considered as potentially useful knob to control quantum systems at zero temperature. The TL liquid example showed how the leading irrelevant operator of the model is related to a phase transition for Rényified state. We would like to understand if similar phenomena can also take place in 2D (Heisenberg models, quantum dimer models, string-net states, ...)

Finally, it may be possible to make more rigorous the arguments of the last chapter concerning continuous symmetry breaking, and to extend them to the case where the subsystem is a line, or when the system has some sharp corners. It would also be interesting to have numerical checks of the prediction that the coefficient of the logarithm depends on the Euler characteristics.

Acknowledgements

I am grateful to all the members of the jury, and the referees in particular, for having accepted this task. I also wish to thank Vincent Pasquier for his collaboration on these subjects, his numerous insightful comments, questions and suggestions. I am also very much indebted to Jean-Marie Stéphan who also contributed in a major way to most of the results reported here. I also want to thank Masaki Oshikawa, Shunsuke Furukawa and Fabien Alet for their collaboration on these problems, or closely related ones.

List of abbreviations

2D	Two spatial dimensions
CFT	Conformal field theory
DMRG	Density matrix renormalization group
EE	Entanglement entropy
ES	Entanglement spectrum
FQHE	Fractional quantum Hall effect
GE	Geometrical entanglement
ICTF	Ising chain in transverse field
LW	Levin-Wen
KP	Kitaev-Preskill
PEPS	Projected entangled pair state
QDM	Quantum dimer model
QFT	Quantum field theory
QMC	Quantum Monte-Carlo
QSL	Quantum spin liquid
RDM	Reduced density matrix
RK	Rokhsar-Kivelson
RVB	Resonating valence-bond
SRE	Shannon-Rényi entropy
TEE	Topological entanglement entropy
TL	Tomonaga-Luttinger

Bibliography

[1] S. Furukawa and G. Misguich, *Topological entanglement entropy in the quantum dimer model on the triangular lattice*, Phys. Rev. B **75**, 214407 (2007), doi:10.1103/PhysRevB.75.214407.

[2] J.-M. Stéphan, S. Furukawa, G. Misguich, and V. Pasquier, *Shannon and entanglement entropies of one- and two-dimensional critical wave functions*, Phys. Rev. B **80**, 184421 (2009), doi:10.1103/PhysRevB.80.184421.

[3] J.-M. Stéphan, G. Misguich, and F. Alet, *Geometric entanglement and Affleck-Ludwig boundary entropies in critical XXZ and Ising chains*, Phys. Rev. B **82**, 180406 (2010), doi:10.1103/PhysRevB.82.180406.

[4] J.-M. Stéphan, G. Misguich, and V. Pasquier, *Rényi entropy of a line in two-dimensional Ising models*, Phys. Rev. B **82**, 125455 (2010), doi:10.1103/PhysRevB.82.125455.

[5] J.-M. Stéphan, G. Misguich, and V. Pasquier, *Phase transition in the Rényi-Shannon entropy of Luttinger liquids*, Phys. Rev. B **84**, 195128 (2011), doi:10.1103/PhysRevB.84.195128.

[6] J.-M. Stéphan, G. Misguich, and V. Pasquier, *Rényi entanglement entropies in quantum dimer models: from criticality to topological order*, J. Stat. Mech. **2012**, P02003 (2012), doi:10.1088/1742-5468/2012/02/P02003.

[7] J. Eisert, M. Cramer, and M. B. Plenio, *Colloquium: Area laws for the entanglement entropy*, Rev. Mod. Phys. **82**, 277 (2010), doi:10.1103/RevModPhys.82.277.

[8] J. D. Bekenstein, *Black Holes and Entropy*, Phys. Rev. D **7**, 2333 (1973), doi:10.1103/PhysRevD.7.2333.

[9] M. B. Hastings, *An area law for one-dimensional quantum systems*, J. Stat. Mech. **2007**, P08024 (2007), doi:10.1088/1742-5468/2007/08/P08024.

[10] S. R. White, *Density matrix formulation for quantum renormalization groups*, Phys. Rev. Lett. **69**, 2863 (1992), doi:10.1103/PhysRevLett.69.2863.

[11] U. Schollwöck, *The density-matrix renormalization group in the age of matrix product states*, Annals of Physics **326**, 96 (2011), doi:10.1016/j.aop.2010.09.012.

[12] E. Stoudenmire and S. R. White, *Studying Two-Dimensional Systems with the Density Matrix Renormalization Group*, Annu. Rev. Condens. Matter Phys. **3**, 111 (2012), doi:10.1146/annurev-conmatphys-020911-125018.

[13] F. Verstraete, M. M. Wolf, D. Perez-Garcia, and J. I. Cirac, *Criticality, the Area Law, and the Computational Power of Projected Entangled Pair States*, Phys. Rev. Lett. **96**, 220601 (2006), doi:10.1103/PhysRevLett.96.220601.

[14] Y.-Y. Shi, L.-M. Duan, and G. Vidal, *Classical simulation of quantum many-body systems with a tree tensor network*, Phys. Rev. A **74**, 022320 (2006), doi:10.1103/PhysRevA.74.022320.

[15] G. Vidal, *Class of Quantum Many-Body States That Can Be Efficiently Simulated*, Phys. Rev. Lett. **101**, 110501 (2008), doi:10.1103/PhysRevLett.101.110501.

[16] C. Holzhey, F. Larsen, and F. Wilczek, *Geometric and renormalized entropy in conformal field theory*, Nucl. Phys. B **424**, 443–467 (1994).

[17] G. Vidal, J. I. Latorre, E. Rico, and A. Kitaev, *Entanglement in Quantum Critical Phenomena*, Phys. Rev. Lett. **90**, 227902 (2003), doi:10.1103/PhysRevLett.90.227902.

[18] P. Calabrese and J. Cardy, *Entanglement entropy and quantum field theory*, J. Stat. Mech.: Theor. Exp. **2004**, P06002 (2004), doi:10.1088/1742-5468/2004/06/P06002.

[19] M. M. Wolf, *Violation of the Entropic Area Law for Fermions*, Phys. Rev. Lett. **96**, 010404 (2006), doi:10.1103/PhysRevLett.96.010404.

[20] E. Fradkin and J. E. Moore, *Entanglement Entropy of 2D Conformal Quantum Critical Points: Hearing the Shape of a Quantum Drum*, Phys. Rev. Lett. **97**, 050404 (2006), doi:10.1103/PhysRevLett.97.050404.

[21] X. G. Wen and Q. Niu, *Ground-state degeneracy of the fractional quantum Hall states in the presence of a random potential and on high-genus Riemann surfaces*, Phys. Rev. B **41**, 9377 (1990), doi:10.1103/PhysRevB.41.9377.

[22] L. Balents, *Spin liquids in frustrated magnets*, Nature **464**, 199 (2010), doi:10.1038/nature08917.

[23] G. Misguich, *Quantum spin liquids*, in J. Jacobsen, S. Ouvry, V. Pasquier, D. Serban, and L. Cugliandolo, editors, Exact Methods in Low-dimensional Statistical Physics and Quantum Computing, volume 89, July 2008 of *Lecture Notes of the Les Houches Summer School*, Oxford University Press (2010), ISBN 978-0199574612.

[24] G. Misguich, *Quantum Spin Liquids and Fractionalization*, in C. Lacroix, P. Mendels, and F. Mila, editors, Introduction to Frustrated Magnetism - Materials, Experiments, Theory, volume 164 of *Springer Series in Solid-State Sciences*, 407–435, Springer Berlin Heidelberg (2011), ISBN 978-3-642-10588-3.

[25] A. Kitaev and J. Preskill, *Topological Entanglement Entropy*, Phys. Rev. Lett. **96**, 110404 (2006), doi:10.1103/PhysRevLett.96.110404.

[26] M. Levin and X.-G. Wen, *Detecting Topological Order in a Ground State Wave Function*, Phys. Rev. Lett. **96**, 110405 (2006), doi:10.1103/PhysRevLett.96.110405.

[27] A. Hamma, R. Ionicioiu, and P. Zanardi, *Bipartite entanglement and entropic boundary law in lattice spin systems*, Phys. Rev. A **71**, 022315 (2005), doi:10.1103/PhysRevA.71.022315.

[28] A. Hamma, R. Ionicioiu, and P. Zanardi, *Ground state entanglement and geometric entropy in the Kitaev model*, Phys. Lett. A **337**, 22 (2005), doi:10.1016/j.physleta.2005.01.060.

[29] Y. Zhang, T. Grover, A. Turner, M. Oshikawa, and A. Vishwanath, *Quasiparticle statistics and braiding from ground-state entanglement*, Phys. Rev. B **85**, 235151 (2012), doi:10.1103/PhysRevB.85.235151.

[30] S. V. Isakov, M. B. Hastings, and R. G. Melko, *Topological entanglement entropy of a Bose-Hubbard spin liquid*, Nat. Phys. **7**, 772 (2011), doi:10.1038/nphys2036.

[31] S. Yan, D. A. Huse, and S. R. White, *Spin-Liquid Ground State of the S = 1/2 Kagome Heisenberg Antiferromagnet*, Science **332**, 1173 (2011), doi:10.1126/science.1201080.

[32] H.-C. Jiang, Z. Wang, and L. Balents, *Identifying topological order by entanglement entropy*, Nat. Phys. **8**, 902 (2012), doi:10.1038/nphys2465.

[33] S. Depenbrock, I. P. McCulloch, and U. Schollwöck, *Nature of the Spin-Liquid Ground State of the S=1/2 Heisenberg Model on the Kagome Lattice*, Phys. Rev. Lett. **109**, 067201 (2012), doi:10.1103/PhysRevLett.109.067201.

[34] S. Nishimoto, N. Shibata, and C. Hotta, *Controlling frustrated liquids and solids with an applied field in a kagome Heisenberg antiferromagnet*, Nat. Commun. **4** (2013), doi:10.1038/ncomms3287.

[35] H. Li and F. D. M. Haldane, *Entanglement Spectrum as a Generalization of Entanglement Entropy: Identification of Topological Order in Non-Abelian Fractional Quantum Hall Effect States*, Phys. Rev. Lett. **101**, 010504 (2008), doi:10.1103/PhysRevLett.101.010504.

[36] X.-L. Qi, H. Katsura, and A. W. W. Ludwig, *General Relationship between the Entanglement Spectrum and the Edge State Spectrum of Topological Quantum States*, Phys. Rev. Lett. **108**, 196402 (2012), doi:10.1103/PhysRevLett.108.196402.

[37] F. Pollmann, A. M. Turner, E. Berg, and M. Oshikawa, *Entanglement spectrum of a topological phase in one dimension*, Phys. Rev. B **81**, 064439 (2010), doi:10.1103/PhysRevB.81.064439.

[38] L. Fidkowski, *Entanglement Spectrum of Topological Insulators and Superconductors*, Phys. Rev. Lett. **104**, 130502 (2010), doi:10.1103/PhysRevLett.104.130502.

[39] D. Poilblanc, *Entanglement Spectra of Quantum Heisenberg Ladders*, Phys. Rev. Lett. **105**, 077202 (2010), doi:10.1103/PhysRevLett.105.077202.

[40] A. M. Läuchli and J. Schliemann, *Entanglement spectra of coupled S=12 spin chains in a ladder geometry*, Phys. Rev. B **85**, 054403 (2012), doi:10.1103/PhysRevB.85.054403.

[41] R. Thomale, A. Sterdyniak, N. Regnault, and B. A. Bernevig, *Entanglement Gap and a New Principle of Adiabatic Continuity*, Phys. Rev. Lett. **104**, 180502 (2010), doi:10.1103/PhysRevLett.104.180502.

[42] A. M. Läuchli, E. J. Bergholtz, J. Suorsa, and M. Haque, *Disentangling Entanglement Spectra of Fractional Quantum Hall States on Torus Geometries*, Phys. Rev. Lett. **104**, 156404 (2010), doi:10.1103/PhysRevLett.104.156404.

[43] P. Calabrese and A. Lefevre, *Entanglement spectrum in one-dimensional systems*, Phys. Rev. A **78**, 032329 (2008), doi:10.1103/PhysRevA.78.032329.

[44] A. M. Läuchli, *Operator content of real-space entanglement spectra at conformal critical points*, arXiv:1303.0741 (2013).

[45] M. A. Metlitski and T. Grover, *Entanglement Entropy of Systems with Spontaneously Broken Continuous Symmetry*, arXiv:1112.5166 (2011).

[46] V. Alba, M. Haque, and A. M. Läuchli, *Entanglement Spectrum of the Two-Dimensional Bose-Hubbard Model*, Phys. Rev. Lett. **110**, 260403 (2013), doi:10.1103/PhysRevLett.110.260403.

[47] Y.-C. He, D. Sheng, and Y. Chen, *Chiral Spin Liquid in a Frustrated Anisotropic Kagome Heisenberg Model*, Phys. Rev. Lett. **112**, 137202 (2014), doi:10.1103/PhysRevLett.112.137202.

[48] S. Ryu and T. Takayanagi, *Holographic Derivation of Entanglement Entropy from the anti–de Sitter Space/Conformal Field Theory Correspondence*, Phys. Rev. Lett. **96**, 181602 (2006), doi:10.1103/PhysRevLett.96.181602.

[49] H. Casini and M. Huerta, *Renormalization group running of the entanglement entropy of a circle*, Phys. Rev. D **85**, 125016 (2012), doi:10.1103/PhysRevD.85.125016.

[50] M. Hermele, T. Senthil, M. P. A. Fisher, P. A. Lee, N. Nagaosa, and X.-G. Wen, *Stability of U(1) spin liquids in two dimensions*, Phys. Rev. B **70**, 214437 (2004), doi:10.1103/PhysRevB.70.214437.

[51] M. Hermele, T. Senthil, and M. P. A. Fisher, *Algebraic spin liquid as the mother of many competing orders*, Phys. Rev. B **72**, 104404 (2005), doi:10.1103/PhysRevB.72.104404.

[52] T. Grover, *Entanglement Monotonicity and the Stability of Gauge Theories in Three Spacetime Dimensions*, Phys. Rev. Lett. **112**, 151601 (2014), doi:10.1103/PhysRevLett.112.151601.

[53] E. Fradkin, D. A. Huse, R. Moessner, V. Oganesyan, and S. L. Sondhi, *Bipartite Rokhsar–Kivelson points and Cantor deconfinement*, Phys. Rev. B **69**, 224415 (2004), doi:10.1103/PhysRevB.69.224415.

[54] D. J. Luitz, F. Alet, and N. Laflorencie, *Universal Behavior beyond Multifractality in Quantum Many-Body Systems*, Phys. Rev. Lett. **112**, 057203 (2014), doi:10.1103/PhysRevLett.112.057203.

[55] M.-C. Chung and I. Peschel, *Density-matrix spectra of solvable fermionic systems*, Phys. Rev. B **64**, 064412 (2001), doi:10.1103/PhysRevB.64.064412.

[56] I. Peschel, *Calculation of reduced density matrices from correlation functions*, J. Phys. A: Math. Gen. **36**, L205–L208 (2003), doi:10.1088/0305-4470/36/14/101.

[57] D. S. Rokhsar and S. A. Kivelson, *Superconductivity and the Quantum Hard-Core Dimer Gas*, Phys. Rev. Lett. **61**, 2376 (1988), doi:10.1103/PhysRevLett.61.2376.

[58] P. W. Leung, K. C. Chiu, and K. J. Runge, *Columnar dimer and plaquette resonating-valence-bond orders in the quantum dimer model*, Phys. Rev. B **54**, 12938 (1996), doi:10.1103/PhysRevB.54.12938.

[59] O. F. Syljuåsen, *Plaquette phase of the square-lattice quantum dimer model: Quantum Monte Carlo calculations*, Phys. Rev. B **73**, 245105 (2006), doi:10.1103/PhysRevB.73.245105.

[60] A. Ralko, D. Poilblanc, and R. Moessner, *Generic Mixed Columnar-Plaquette Phases in Rokhsar-Kivelson Models*, Phys. Rev. Lett. **100**, 037201 (2008), doi:10.1103/PhysRevLett.100.037201.

[61] E. Ardonne, P. Fendley, and E. Fradkin, *Topological order and conformal quantum critical points*, Ann. Phys. **310**, 493 (2004), doi:10.1016/j.aop.2004.01.004.

[62] C. L. Henley, *From classical to quantum dynamics at Rokhsar–Kivelson points*, J. Phys.: Condens. Matter **16**, S891 (2004), doi:10.1088/0953-8984/16/11/045.

[63] C. Castelnovo, C. Chamon, C. Mudry, and P. Pujol, *From quantum mechanics to classical statistical physics: Generalized Rokhsar–Kivelson Hamiltonians and the "Stochastic Matrix Form" decomposition*, Ann. Phys. **318**, 316 (2005), doi:10.1016/j.aop.2005.01.006.

[64] M. B. Hastings, I. González, A. B. Kallin, and R. G. Melko, *Measuring Rényi Entanglement Entropy in Quantum Monte Carlo Simulations*, Phys. Rev. Lett. **104**, 157201 (2010), doi:10.1103/PhysRevLett.104.157201.

[65] P. Kasteleyn, *The statistics of dimers on a lattice*, Physica **27**, 1209–1225 (1961).

[66] M. E. Fisher, *Statistical Mechanics of Dimers on a Plane Lattice*, Phys. Rev. **124**, 1664 (1961), doi:10.1103/PhysRev.124.1664.

[67] P. W. Anderson, *Resonating valence bonds: A new kind of insulator?*, Mat. Res. Bull. **8**, 153 (1973), doi:10.1016/0025-5408(73)90167-0.

[68] P. W. Anderson, *The Resonating Valence Bond State in La2CuO4 and Superconductivity*, Science **235**, 1196 (1987), doi:10.1126/science.235.4793.1196.

[69] P. Lecheminant, B. Bernu, C. Lhuillier, L. Pierre, and P. Sindzingre, *Order versus disorder in the quantum Heisenberg antiferromagnet on the kagomé lattice using exact spectra analysis*, Phys. Rev. B **56**, 2521 (1997), doi:10.1103/PhysRevB.56.2521.

[70] G. Misguich, B. Bernu, C. Lhuillier, and C. Waldtmann, *Spin Liquid in the Multiple-Spin Exchange Model on the Triangular Lattice: 3He on Graphite*, Phys. Rev. Lett. **81**, 1098 (1998), doi:10.1103/PhysRevLett.81.1098.

[71] G. Misguich, C. Lhuillier, B. Bernu, and C. Waldtmann, *Spin-liquid phase of the multiple-spin exchange Hamiltonian on the triangular lattice*, Phys. Rev. B **60**, 1064 (1999), doi:10.1103/PhysRevB.60.1064.

[72] N. Read and S. Sachdev, *Large-N expansion for frustrated quantum antiferromagnets*, Phys. Rev. Lett. **66**, 1773 (1991), doi:10.1103/PhysRevLett.66.1773.

[73] S. Sachdev, *Kagome- and triangular-lattice Heisenberg antiferromagnets: Ordering from quantum fluctuations and quantum-disordered ground states with unconfined bosonic spinons*, Phys. Rev. B **45**, 12377 (1992), doi:10.1103/PhysRevB.45.12377.

[74] R. Moessner and S. L. Sondhi, *Resonating Valence Bond Phase in the Triangular Lattice Quantum Dimer Model*, Phys. Rev. Lett. **86**, 1881 (2001), doi:10.1103/PhysRevLett.86.1881.

[75] A. Ralko, M. Ferrero, F. Becca, D. Ivanov, and F. Mila, *Zero-temperature properties of the quantum dimer model on the triangular lattice*, Phys. Rev. B **71**, 224109 (2005), doi:10.1103/PhysRevB.71.224109.

[76] A. Ralko, M. Ferrero, F. Becca, D. Ivanov, and F. Mila, *Dynamics of the quantum dimer model on the triangular lattice: Soft modes and local resonating valence-bond correlations*, Phys. Rev. B **74**, 134301 (2006), doi:10.1103/PhysRevB.74.134301.

[77] A. Ralko, M. Ferrero, F. Becca, D. Ivanov, and F. Mila, *Crystallization of the resonating valence bond liquid as vortex condensation*, Phys. Rev. B **76**, 140404 (2007), doi:10.1103/PhysRevB.76.140404.

[78] J. S. Helton, K. Matan, M. P. Shores, E. A. Nytko, B. M. Bartlett, Y. Yoshida, Y. Takano, A. Suslov, Y. Qiu, J.-H. Chung, D. G. Nocera, and Y. S. Lee, *Spin Dynamics of the Spin-1/2 Kagome Lattice Antiferromagnet ZnCu3(OH)6Cl2*, Phys. Rev. Lett. **98**, 107204 (2007), doi:10.1103/PhysRevLett.98.107204.

[79] P. Mendels, F. Bert, M. A. de Vries, A. Olariu, A. Harrison, F. Duc, J. C. Trombe, J. S. Lord, A. Amato, and C. Baines, *Quantum Magnetism in the Paratacamite Family: Towards an Ideal Kagomé Lattice*, Phys. Rev. Lett. **98**, 077204 (2007), doi:10.1103/PhysRevLett.98.077204.

[80] Y. Shimizu, K. Miyagawa, K. Kanoda, M. Maesato, and G. Saito, *Spin Liquid State in an Organic Mott Insulator with a Triangular Lattice*, Phys. Rev. Lett. **91**, 107001 (2003), doi:10.1103/PhysRevLett.91.107001.

[81] R. Masutomi, Y. Karaki, and H. Ishimoto, *Gapless Spin Liquid Behavior in Two-Dimensional Solid He3*, Phys. Rev. Lett. **92**, 025301 (2004), doi:10.1103/PhysRevLett.92.025301.

[82] E. Lieb, T. Schultz, and D. Mattis, *Two soluble models of an antiferromagnetic chain*, Ann. Phys. **16**, 407 (1961), doi:10.1016/0003-4916(61)90115-4.

[83] M. B. Hastings, *Lieb-Schultz-Mattis in higher dimensions*, Phys. Rev. B **69**, 104431 (2004), doi:10.1103/PhysRevB.69.104431.

[84] M. Oshikawa, *Commensurability, Excitation Gap, and Topology in Quantum Many-Particle Systems on a Periodic Lattice*, Phys. Rev. Lett. **84**, 1535 (2000), doi:10.1103/PhysRevLett.84.1535.

[85] B. Nachtergaele and R. Sims, *A Multi-Dimensional Lieb-Schultz-Mattis Theorem*, Commun. Math. Phys. **276**, 437 (2007), doi:10.1007/s00220-007-0342-z.

[86] X. G. Wen, *Vacuum degeneracy of chiral spin states in compactified space*, Phys. Rev. B **40**, 7387 (1989), doi:10.1103/PhysRevB.40.7387.

[87] X. G. Wen, *Mean-field theory of spin-liquid states with finite energy gap and topological orders*, Phys. Rev. B **44**, 2664 (1991), doi:10.1103/PhysRevB.44.2664.

[88] M. Oshikawa and T. Senthil, *Fractionalization, Topological Order, and Quasiparticle Statistics*, Phys. Rev. Lett. **96**, 060601 (2006), doi:10.1103/PhysRevLett.96.060601.

[89] S.-A. Cheong and C. L. Henley, *Correlation density matrix: An unbiased analysis of exact diagonalizations*, Phys. Rev. B **79**, 212402 (2009), doi:10.1103/PhysRevB.79.212402.

[90] M. M. Wolf, F. Verstraete, M. B. Hastings, and J. I. Cirac, *Area Laws in Quantum Systems: Mutual Information and Correlations*, Phys. Rev. Lett. **100**, 070502 (2008), doi:10.1103/PhysRevLett.100.070502.

[91] M. A. Levin and X.-G. Wen, *String-net condensatsion: A physical mechanism for topological phasesZ*, Phys. Rev. B **71**, 045110 (2005), doi:10.1103/PhysRevB.71.045110.

[92] G. Misguich, D. Serban, and V. Pasquier, *Quantum Dimer Model on the Kagome Lattice: Solvable Dimer-Liquid and Ising Gauge Theory*, Phys. Rev. Lett. **89**, 137202 (2002), doi:10.1103/PhysRevLett.89.137202.

[93] I. Affleck and A. W. W. Ludwig, *Universal noninteger "ground-state degeneracy" in critical quantum systems*, Phys. Rev. Lett. **67**, 161 (1991), doi:10.1103/PhysRevLett.67.161.

[94] P. Fendley, R. Moessner, and S. L. Sondhi, *Classical dimers on the triangular lattice*, Phys. Rev. B **66**, 214513 (2002), doi:10.1103/PhysRevB.66.214513.

[95] A. Ioselevich, D. A. Ivanov, and M. V. Feigelman, *Ground-state properties of the Rokhsar-Kivelson dimer model on the triangular lattice*, Phys. Rev. B **66**, 174405 (2002), doi:10.1103/PhysRevB.66.174405.

[96] S. Furukawa, G. Misguich, and M. Oshikawa, *Reduced density matrices and topological order in a quantum dimer model*, J. Phys.: Condens. Matter **19**, 145212 (2007), doi:10.1088/0953-8984/19/14/145212.

[97] M. Haque, O. Zozulya, and K. Schoutens, *Entanglement Entropy in Fermionic Laughlin States*, Phys. Rev. Lett. **98**, 060401 (2007), doi:10.1103/PhysRevLett.98.060401.

[98] Y. Zhang, T. Grover, and A. Vishwanath, *Topological entanglement entropy of Z2 spin liquids and lattice Laughlin states*, Phys. Rev. B **84**, 075128 (2011), doi:10.1103/PhysRevB.84.075128.

[99] S. T. Flammia, A. Hamma, T. L. Hughes, and X.-G. Wen, *Topological Entanglement Rényi Entropy and Reduced Density Matrix Structure*, Phys. Rev. Lett. **103**, 261601 (2009), doi:10.1103/PhysRevLett.103.261601.

[100] M. Kac, *Can One Hear the Shape of a Drum?*, Amer. Math. Monthly **73**, 1 (1966), doi:10.2307/2313748.

[101] J. L. Cardy and I. Peschel, *Finite-size dependence of the free energy in two-dimensional critical systems*, Nucl. Phys. B **300**, 377 (1988), doi:10.1016/0550-3213(88)90604-9.

[102] R. G. Melko, A. B. Kallin, and M. B. Hastings, *Finite-size scaling of mutual information in Monte Carlo simulations: Application to the spin-12 XXZ model*, Phys. Rev. B **82**, 100409 (2010), doi:10.1103/PhysRevB.82.100409.

[103] R. R. P. Singh, M. B. Hastings, A. B. Kallin, and R. G. Melko, *Finite-Temperature Critical Behavior of Mutual Information*, Phys. Rev. Lett. **106**, 135701 (2011), doi:10.1103/PhysRevLett.106.135701.

[104] J. Wilms, J. Vidal, F. Verstraete, and S. Dusuel, *Finite-temperature mutual information in a simple phase transition*, J. Stat. Mech. **2012**, P01023 (2012), doi:10.1088/1742-5468/2012/01/P01023.

[105] J. Wilms, M. Troyer, and F. Verstraete, *Mutual information in classical spin models*, J. Stat. Mech. **2011**, P10011 (2011), doi:10.1088/1742-5468/2011/10/P10011.

[106] H. W. Lau and P. Grassberger, *Information theoretic aspects of the two-dimensional Ising model*, Phys. Rev. E **87**, 022128 (2013), doi:10.1103/PhysRevE.87.022128.

[107] J. Iaconis, S. Inglis, A. B. Kallin, and R. G. Melko, *Detecting classical phase transitions with Renyi mutual information*, Phys. Rev. B **87**, 195134 (2013), doi:10.1103/PhysRevB.87.195134.

[108] A. Rahmani and G.-W. Chern, *Universal Rényi mutual information in classical systems: The case of kagome ice*, Phys. Rev. B **88**, 054426 (2013), doi:10.1103/PhysRevB.88.054426.

[109] H. W. J. Blote and H. J. Hilhorst, *Roughening transitions and the zero-temperature triangular Ising antiferromagnet*, J. Phys. A: Math. Gen. **15**, L631 (1982), doi:10.1088/0305-4470/15/11/011.

[110] F. Alet, Y. Ikhlef, J. L. Jacobsen, G. Misguich, and V. Pasquier, *Classical dimers with aligning interactions on the square lattice*, Phys. Rev. E **74**, 041124 (2006), doi:10.1103/PhysRevE.74.041124.

[111] J.-M. Stéphan, *Thèse Jean-Marie Stéphan*, Ph.D. thesis, Université Paris-Sud 11 (2011).

[112] J.-M. Stéphan, *Shannon and Rényi mutual information in quantum critical spin chains*, arXiv:1403.6157 (2014).

[113] F. Alet, J. L. Jacobsen, G. Misguich, V. Pasquier, F. Mila, and M. Troyer, *Interacting Classical Dimers on the Square Lattice*, Phys. Rev. Lett. **94**, 235702 (2005), doi:10.1103/PhysRevLett.94.235702.

[114] D. J. Luitz, N. Laflorencie, and F. Alet, *Participation spectroscopy and entanglement Hamiltonian of quantum spin models*, arXiv:1404.3717 (2014).

[115] F. Evers and A. D. Mirlin, *Anderson transitions*, Rev. Mod. Phys. **80**, 1355 (2008), doi:10.1103/RevModPhys.80.1355.

[116] Y. Y. Atas and E. Bogomolny, *Multifractality of eigenfunctions in spin chains*, Phys. Rev. E **86**, 021104 (2012), doi:10.1103/PhysRevE.86.021104.

[117] M. P. Zaletel, J. H. Bardarson, and J. E. Moore, *Logarithmic Terms in Entanglement Entropies of 2D Quantum Critical Points and Shannon Entropies of Spin Chains*, Phys. Rev. Lett. **107**, 020402 (2011), doi:10.1103/PhysRevLett.107.020402.

[118] F. C. Alcaraz and M. A. Rajabpour, *Universal Behavior of the Shannon Mutual Information of Critical Quantum Chains*, Phys. Rev. Lett. **111**, 017201 (2013), doi:10.1103/PhysRevLett.111.017201.

[119] I. Affleck, *Field Theory Methods and Quantum Critical Phenomena*, in E. Brézin and J. Zinn-Justin, editors, Fields, Strings and Critical Phenomena, Proceedings of Les Houches Summer School, 1988, 563, North Holland Publishing, Amsterdam (1990).

[120] P. Fendley, H. Saleur, and N. P. Warner, *Exact solution of a massless scalar field with a relevant boundary interaction*, Nucl. Phys. B **430**, 577–596 (1994), doi:10.1016/0550-3213(94)90160-0.

[121] D. Schwandt, F. Alet, and M. Oshikawa, *Valence bond distribution and correlation in bipartite Heisenberg antiferromagnets*, Phys. Rev. B **89**, 104416 (2014), doi:10.1103/PhysRevB.89.104416.

[122] M. Oshikawa, *Boundary Conformal Field Theory and Entanglement Entropy in Two-Dimensional Quantum Lifshitz Critical Point*, arXiv:1007.3739 (2010).

[123] J. L. Cardy, *Conformal invariance and surface critical behavior*, Nucl. Phys. B **240**, 514 (1984), doi:10.1016/0550-3213(84)90241-4.

[124] C. G. Callan, I. R. Klebanov, A. W. W. Ludwig, and J. M. Maldacena, *Exact solution of a boundary conformal field theory*, Nucl. Phys. B **422**, 417 (1994), doi:10.1016/0550-3213(94)90440-5.

[125] Y. Kumano, G. Misguich, and M. Oshikawa, *Correlations and Luttinger parameter in the "Rényified" ground state of XXZ spin chains*, In preparation (2014).

[126] J. I. Cirac and G. Sierra, *Infinite matrix product states, conformal field theory, and the Haldane-Shastry model*, Phys. Rev. B **81**, 104431 (2010), doi:10.1103/PhysRevB.81.104431.

[127] J. Sawada, *Generating Bracelets in Constant Amortized Time*, SIAM J. on Comp. **31**, 259 (2001), doi:10.1137/S0097539700377037.

[128] J. L. Cardy, *Effect of boundary conditions on the operator content of two-dimensional conformally invariant theories*, Nucl. Phys. B **275**, 200 (1986), doi:10.1016/0550-3213(86)90596-1.

[129] J. L. Cardy, *Boundary conditions, fusion rules and the Verlinde formula*, Nucl. Phys. B **324**, 581 (1989), doi:10.1016/0550-3213(89)90521-X.

[130] M. Oshikawa and I. Affleck, *Defect Lines in the Ising Model and Boundary States on Orbifolds*, Phys. Rev. Lett. **77**, 2604 (1996), doi:10.1103/PhysRevLett.77.2604.

[131] T.-C. Wei and P. M. Goldbart, *Geometric measure of entanglement and applications to bipartite and multipartite quantum states*, Phys. Rev. A **68**, 042307 (2003), doi:10.1103/PhysRevA.68.042307.

[132] T.-C. Wei, D. Das, S. Mukhopadyay, S. Vishveshwara, and P. M. Goldbart, *Global entanglement and quantum criticality in spin chains*, Phys. Rev. A **71**, 060305 (2005), doi:10.1103/PhysRevA.71.060305.

[133] Q.-Q. Shi, R. Orús, J. O. Fjærestad, and H.-Q. Zhou, *Finite-size geometric entanglement from tensor network algorithms*, New J. Phys. **12**, 025008 (2010), doi:10.1088/1367-2630/12/2/025008.

[134] H. F. Song, N. Laflorencie, S. Rachel, and K. Le Hur, *Entanglement entropy of the two-dimensional Heisenberg antiferromagnet*, Phys. Rev. B **83**, 224410 (2011), doi:10.1103/PhysRevB.83.224410.

[135] A. B. Kallin, M. B. Hastings, R. G. Melko, and R. R. P. Singh, *Anomalies in the entanglement properties of the square-lattice Heisenberg model*, Phys. Rev. B **84**, 165134 (2011), doi:10.1103/PhysRevB.84.165134.

[136] D. J. Luitz, F. Alet, and N. Laflorencie, *Shannon-Rényi entropies and participation spectra across three-dimensional O(3) criticality*, Phys. Rev. B **89**, 165106 (2014), doi:10.1103/PhysRevB.89.165106.

[137] B. Duplantier and F. David, *Exact partition functions and correlation functions of multiple Hamiltonian walks on the Manhattan lattice*, J. Stat. Phys. **51**, 327 (1988), doi:10.1007/BF01028464.

[138] B. Osgood, R. Phillips, and P. Sarnak, *Extremals of determinants of Laplacians*, J. Funct. Anal. **80**, 148 (1988), doi:10.1016/0022-1236(88)90070-5.

[139] P. W. Anderson, *An Approximate Quantum Theory of the Antiferromagnetic Ground State*, Phys. Rev. **86**, 694 (1952), doi:10.1103/PhysRev.86.694.

[140] B. Bernu, C. Lhuillier, and L. Pierre, *Signature of Néel order in exact spectra of quantum antiferromagnets on finite lattices*, Phys. Rev. Lett. **69**, 2590 (1992), doi:10.1103/PhysRevLett.69.2590.

[141] C. Lhuillier, *Frustrated Quantum Magnets*, cond-mat/0502464 (2005).

[142] E. Lieb and D. Mattis, *Ordering Energy Levels of Interacting Spin Systems*, J. Math. Phys. **3**, 749 (1962).